

Unlock the energy flexibility resources of zero-emission vehicles to simultaneously alleviate the negative impact on grid and traffic between remote buildings with predictive controls[☆]

Zhenyu Dou ^{a,*}, Kai Pan ^c, Yang Xu ^d, Sunliang Cao ^{a,b,e,*}

^a Renewable Energy Research Group (RERG), Department of Building Environment and Energy Engineering, Faculty of Construction and Environment, The Hong Kong Polytechnic University, Kowloon, Hong Kong Special Administrative Region

^b Research Institute for Smart Energy (RISE), The Hong Kong Polytechnic University, Kowloon, Hong Kong Special Administrative Region

^c Department of Logistics and Maritime Studies, Faculty of Business, The Hong Kong Polytechnic University, Kowloon, Hong Kong Special Administrative Region

^d Department of Land Surveying and Geo-Informatics, The Hong Kong Polytechnic University, Kowloon, Hong Kong Special Administrative Region

^e Research Institute for Sustainable Urban Development (RISUD), The Hong Kong Polytechnic University, Kowloon, Hong Kong Special Administrative Region

HIGHLIGHTS

- Unlock energy flexibility of zero-emission vehicles for carbon-neutral communities.
- Energy synergies between the zero-energy transportation, building, grid and traffic.
- Utilizing EVs for remote energy sharing while reducing negative impact on traffic.
- Simultaneous alleviation of negative impact of EV charging on grid and traffic.
- Model predictive controls for advanced energy management of zero-emission vehicles.

ARTICLE INFO

Keywords:

Zero-emission vehicles
EV-based energy flexibility
Traffic congestion impact
Grid stability
Energy sharing
Carbon-neutral community

ABSTRACT

To mitigate the climate change caused by carbon emission issues, zero-emission vehicles (ZEVs) and zero-energy buildings (ZEBs) have attracted increasing attention due to the significant proportion of energy-related carbon emissions from the transportation and building sectors. The energy-matching problem of ZEBs between demand and generation is widely noticed by academia, and the energy-sharing method using electric vehicles (EVs) has proved to be an effective approach to improve energy-matching performance. However, the stability issue of the grid-interaction performance caused by the unstable renewable energy generation and the negative impact on the road traffic of ZEVs for energy sharing receive limited attention. This paper proposes instantaneous and predictive control methods for a zero-emission system consisting of two zero-energy buildings using ZEV energy sharing to enhance the building-grid interaction stability and reduce the negative impact of ZEVs on road congestion. A genetic algorithm model is implemented in predictive control. The impacts of different ocean renewable energy types on energy matching, grid stability, and economic benefits are investigated. The results show that the instantaneous control can provide up to 71.0 % better grid-interaction stability performance than basic control. An average of 9.2 % enhancement in the stability performance can be further achieved after implementing genetic predictive control. When considering road impact in predictive control, the annual practical road impact changes from around -0.16 to around 0.13 to 0.15 under different scenarios, while the grid-interaction stability performance remains almost the same with the genetic predictive control that just considers grid stability.

[☆] This article is part of a Special issue entitled: 'Low-Carbon Transport(Wen-Long Shang)' published in Applied Energy.

* Corresponding authors at: Renewable Energy Research Group (RERG), Department of Building Environment and Energy Engineering, Faculty of Construction and Environment, The Hong Kong Polytechnic University, Kowloon, Hong Kong Special Administrative Region.

E-mail addresses: zhenyu.dou@connect.polyu.hk (Z. Dou), sunliang.cao@polyu.edu.hk, caosunliang@msn.com (S. Cao).

Nomenclature	
B2V	Building to vehicle function
B _{hotel_exp}	Grid-interaction benchmark for hotel exported power (kW)
B _{hotel_imp}	Grid-interaction benchmark for hotel imported power (kW)
B _{office_exp}	Grid-interaction benchmark for office exported power (kW)
B _{office_imp}	Grid-interaction benchmark for office imported power (kW)
CE _a	The annual carbon dioxide emission of the whole system (kg CO ₂ , eq)
CEF _{eg}	The equivalent factor of carbon dioxide emissions of the electric grid (kg CO ₂ , eq/kWh)
C _{imp_save}	The bill reduction for the stakeholder because of the saved imported energy
C _{O&M}	The operation and maintenance cost
C _{Ree}	Income from FiT subsidies for electricity generation by renewable energy system
C _{repl}	The replacement cost
C _{sv}	The salvage value of batteries
E _{direct, sys}	The annual direct net energy imported from the electric grid of the whole system (kWh)
EV	Electric vehicle
FiT	Feed-in Tariff
FPV	Floating Photovoltaic
FSOC	Fractional state of charge
I _{Ree}	The initial investment for the renewable energy system installation
L _{elec, sys}	The total power of the electrical demand of the whole system (kW)
NPV _{rel}	Relative net present value
NRI	Negative road impact
OEF _e	On-site electrical energy fraction
OEM _e	On-site electrical energy matching
ORI	Overall road impact
OWT	Offshore Wind Turbine
P _{EV, sys}	The power of electricity to the building-integrated EV system (kW)
P _{excess}	The excessive power compared between local renewable energy generation and demand (kW)
P _{exp}	The electrical power exported to the external grid (kW)
P _{imp}	The electrical power imported from the external grid (kW)
P _{REE, sys}	The power of electricity produced by renewable energy systems of the whole system (kW)
PRI	Positive road impact
P _{shortage}	The shortage of power compared between local renewable energy generation and demand (kW)
REe	Renewable electricity
σ _{imp_hotel}	Standard deviation of hotel annual imported power
σ _{imp_office}	Standard deviation of office annual imported power
σ _{exp_hotel}	Standard deviation of hotel annual exported power
σ _{exp_office}	Standard deviation of office annual exported power
TSG	Tidal Stream Generator
V2B	Vehicle to building function
WMI	Weighted Matching Index
WSI	Weighted Stability Index
ZEB	Zero-energy/emission building

1. Introduction and background

Nowadays, carbon emission issues have attracted increasing attention worldwide due to climate change. Many countries and regions have published goals to reduce carbon emissions and increase the utilization of non-fossil sources. The U.S. has set a goal of reducing net greenhouse gas emissions to zero by 2050 at the latest [1]. China has also announced ‘Dual carbon’ goals in its Nations Determined Contributions (NDCs), aiming to achieve its peak carbon emissions and carbon neutrality before 2030 and 2060 respectively [2]. Reducing carbon emissions in both the transportation and building sectors is essential to meet these goals. First, the transportation sector accounts for around 24 % of the global emissions of energy-related carbon dioxide [3,4], and road transportation accounts for three-quarters of them [4]. Achieving a carbon-neutral transportation system is an indispensable part of achieving a carbon-neutral community. Second, as reported by the World Green Building Council, the construction and building sectors account for 37 % of global energy-related carbon emissions [5]. Hence, the conception of zero-emission building (ZEB) attracts growing interest due to its environmental and economic benefits. A zero-emission building (ZEB) is commonly recognized as a building that achieves carbon neutrality through the implementation of local systems generating renewable energy, such as photovoltaic panels or wind turbines; these systems can provide sufficient energy to offset the carbon footprint associated with energy usage and material consumption of the building [6]. There is a common problem among these renewable energy generation systems: the instability caused by weather dependency, by which these systems do not provide stable energy sources for fulfilling the demand of a building consistently. So, integrating the internal energy system with the public electricity grid is essential for a ZEB, which allows a ZEB to import electricity when there is an energy shortage and to export excessive renewable energy. This integrated ZEB-Grid system has

two issues that need to be considered. One is the matching between the energy demand and renewable energy generation, which is important to the design of renewable energy generation and its storage system. The other is the interactive performance between ZEB and the external grid. ZEB has a negative impact on the grid because of the instability of renewable energy generation [7], contributing to unexpected instantaneous grid load fluctuation.

In academia, observing the challenges of the matching problem of ZEB between renewable energy generation and building demand, some researchers focused on introducing electric vehicles (EVs) as mobile batteries into ZEB-Grid systems to balance the on-site energy generation and demand. Doroudchi et al. [8] integrated an EV with a 24 kWh battery capacity as an active component into a three-stories-building energy system with Photovoltaic (PV) panels installed. They investigated the impact of EVs on the performance in energy matching of the studied system by using two indicators (OEF and OEM) [9] for system energy-matching performance evaluation. Their findings showed that by activating the building to EV to building function, the energy-matching performance was improved with 27 % and 12 % enhancement of OEF and OEM respectively [8]. Barone et al. [10] examined the technical and economic impact of a microgrid consisting of two different buildings with PV panels installed, a stationary battery, and an EV as an energy vector. Their results showed that with the bidirectional exchange function of EVs, the utilization of on-site energy generation could reach 57.8 % [10]. Huang et al. [11] developed a coordinated control with smart EV charging and discharging strategies to optimize the energy performance of a building cluster consisting of three separate buildings with potential PV panels installation. The results of the study showed that the daily self-consumption rates of renewable energy could be improved by 19 % by using smart EV control and energy sharing [11]. Barone et al. [12] investigated the capability of EVs to serve as resources for energy storage and transmission to increase the on-site renewable

energy utilization of building clusters powered by PV panels. They simulated in twenty-two European cities, and their analyses indicated that the self-consumption of renewable energy increased significantly with reductions of the imported energy from the external grid ranging from 13 % to 71 % [12]. In addition to solar energy-powered ZEB, the impacts of EVs on ZEB energy systems with other energy sources were also investigated. Cao [13] compared the impacts on energy and environmental aspects of introducing an H2 vehicle and an EV into a ZEB powered by PV panels or wind turbines. In his study, the monthly imported and exported energy were both reduced by 0.7–1.7 kWh/m² and 0.9–1.6 kWh/m², respectively, by relieving the FSOC limitation from 0.95 to 0.5 [13]. Cao [14] also expanded the mobile boundary of EVs to remote charging stations and investigated its enhancement in the technical performance of the zero-energy system consisting of an office building, BIPVs, and wind turbines. His results showed that the boundary expansion could significantly enhance energy-matching capacities with both OEM and OEF at 62 % [14]. Zhou et al. [15] examined the energy flexibility of a residential ZEB with BIPVs, wind turbines, and thermal energy storage, integrated with an electric vehicle. Their findings indicated that renewable energy could cover 87.2 % of the annual electricity charged to EVs and 71.7 % of the charged energy could be utilized for supporting the building electricity load [15]. Liu et al. [16] implemented an integrated energy-sharing approach with micro-grid and electric vehicles in a scenario with neighboring ZEBs and achieved around 7 % enhancement in energy-matching performance [16]. Fachrizal et al. [17] expanded the scale of zero-energy systems to urban scale and studied the improvement brought by smart EV charging and the function of vehicle-to-grid on the performance in energy matching aspect of a zero-energy urban area supported by wind-PV production. It was observed that the performance of the city in load matching was improved from 68 % to 84 % [17].

Meanwhile, many researchers have been studying the grid stability issues brought about by the instability of grid-connected renewable energy systems and EV charging. Shafiqullah et al. [18] reviewed the challenges of integrating solar PV systems into grids. In the work, the authors demonstrated that there would be both voltage and angular stability issues in grid-connected PV systems [18]. Eftekharnejad et al. [19] studied the impact of energy generation by PV panels on power systems. The results showed that the stability performance of the grid in both steady and transient states would be influenced by increasing penetration of PV generation [19]. Alquthami et al. [20] examined the impact of the PV generation change caused by solar radiation and temperature changes on the power system stability. The study demonstrated an unsafe area of irradiance change rate, higher than 125 W/m²·s caused by cloud cover, etc. [20]. This unsafe irradiance changing rate would result in an unacceptable change in PV power generation and the power system operator would not have enough time to respond [20]. There are also similar stability issues occurring on grid-connected wind turbines. He et al. [21] examined the impacts of the implementation of three different models of wind turbines on the stability performance of power systems. In this study, the authors indicated that the stability performance decrease of the power system is influenced by the penetration level of wind turbine generators [21]. Adetokun et al. [22] assessed the stability performance in voltage of an electric grid with different penetration levels of wind energy. Their results showed that some grid loadability enhancement measures should be implemented to increase the penetration level of wind turbines [22]. Schmietendorf et al. [23] implemented two kinds of intermittent noises on a power grid to model the impact of turbulent wind energy on the grid. They found that the implementation of wind energy and the instability of wind can destabilize the grid and simultaneously decrease the voltage and frequency quality [23]. In the kind of ZEBs integrated with electric vehicles, the instability of grid interaction not only comes from renewable energy systems but also is brought by EV charging behavior inside the buildings. Onar et al. [24] studied the impact of the penetration of EVs with plug-in hybrid energy format on the stability performance of the

grid network. They modeled a 3-bus IEEE test system and investigated its power system and the stability performance in voltage. Their results showed that the distribution network integrated with EVs is more delicate when facing the power system disturbance and takes more time to recover to the pre-disruption steady state [24]. Sayed et al. [25] proposed a dynamic attack model for EVs to test the impact on grid instability. The results showed that under the developed attack model, the grid generators can be tripped even with 6.6 % of the total load [25]. To improve the transient stability performance of the grid with EVs, Wu et al. [26] proposed a hybrid power system integrated with superconducting magnetic energy storage and grid-supported electric vehicles and investigated the transient system stability. They found that the transient stability and dynamic performance can be improved by simultaneously implementing SEMS and activating the vehicle-to-grid function of EVs [26]. Dharmakeerthi et al. [27] developed a static load model for EV charging to assess the impact of fast charging behaviors of EVs on the stability performance in voltage of the grid operation. Their findings showed that the integration with fast charging stations can bring over 50 % reduction in the loading margin of steady state to the power grid [27].

Some recent studies highlighted the negative impact on road congestion of EV charging and commuting behaviors. Grigorev et al. [28] proposed a modeling approach comprised of a traffic simulation model and a queueing model for charging stations and investigated the impact of increasing EV penetration levels on traffic congestion and energy consumption. The study illustrated that the total travel time of all vehicles would be increased by 4.9 % when the EV penetration reaches 5 % [28]. Rigas et al. [29] tried to manage the urban EV charging behavior through proposed centralized and decentralized approaches. Their study found that the centralized mechanism can manage the congestion best, but it is unsuitable for different scales [29]. The impact of EVs on congestion is also influenced by the battery capacity, affecting the path choice [30]. Jing et al. investigated the congestion patterns of EVs restricted by the battery capacity and proposed a mathematical model for stochastic traffic assignments [30]. Marmaras et al. [31] developed a multi-agent simulator to simulate the EV driver's behavior in road traffic. By considering unaware and aware behavioral profiles, they found that the aware EV agents who would consider the real road information can significantly reduce congestion compared with unaware EV agents who always chose the shortest route [31]. The study conducted by Wang et al. [32] indicated that the penetration of EVs would result in extra congestion during morning commute. Two intervention methods, including separating EVs and congestion charging are proposed in this study to alleviate the effects of EVs on congestion [32]. Wang et al. [33] proposed an EV corridor model and implemented the model for traffic management and charging station optimization. The fixed arrival time would be released to a time window for arriving at a certain destination by implementing the proposed model [33]. Cen et al. [34] proposed a mixed model with both EVs and GVs (Gasoline Vehicles) considering the charging behavior of EVs for commute trips in urban areas with a concept called EV charging ratio, providing an approach for EV adoption strategies optimization. Huang et al. [35] introduced support vector regression to EV traffic management and developed a congestion prevention approach for normal and autonomous EVs. Their study showed that EVs have significant potential to reduce road congestion under appropriate control methods [35].

From the reviews of the literature mentioned above, it can be identified that there are some scientific gaps in the following aspects of the international academic community:

First, most existing research on the energy-sharing control for ZEBs integrated with electric vehicles focused on enhancing energy-matching performance. However, limited studies paid attention to the grid interaction instability issue caused by renewable energy generation and zero-emission vehicle (ZEV) charging of this kind of hybrid system. This results in a lack of knowledge of the grid-interactive performance and control strategies for stabilizing the grid interaction.

Second, limited analyses of the negative impact on road congestion have been conducted for the energy-sharing studies using zero-emission vehicles between several ZEBs. Increasing EV penetration levels challenges road congestion conditions. Energy sharing using EVs between ZEBs would bring additional pressure on traffic, and the specific impact analysis and feasible control approach to minimize this kind of negative road impact have not been investigated.

Third, most controls developed for this kind of carbon-neutral hybrid system consisting of ZEBs and zero-emission vehicles are based on instantaneous information. This may result in limitations on the system performance. Predictive control methods need to be developed to utilize the predicted information in the future of the system to provide a better performance than the instantaneous controls.

In response to the abovementioned scientific gaps, this study focuses on proposing instantaneous control and advanced predictive control methods for two zero-energy buildings to use ZEV energy sharing for enhancing the building-grid interaction stability and reducing the negative impact of ZEVs on road congestion. For instantaneous control, an innovative parameter for stability benchmark is proposed and the impacts of different kinds of renewable energy systems and different benchmarks on the system's techno-economic performance are comprehensively analyzed. An advanced genetic algorithm is introduced by using historical demand data to conduct predictive control for grid stability. At the base of genetic predictive control, a predictive control method using averaged historical road congestion information is also integrated, and the impact of different averaging levels of historical road data on the performance of predictive control is further analyzed. In Section 2 following this introduction, the weather conditions, demands of buildings and vehicles, together with the simulation environment, are briefly introduced. In Section 3, the detailed buildings and integrated ZEV system are discussed including the renewable energy systems and the strategies for the proposed instantaneous and predictive

controls, followed by the analysis criteria introduced in Section 4. The results and corresponding analysis for the proposed controls are discussed in Section 5. In Section 6, the conclusions of this study are presented.

2. Weather, and demands of buildings and vehicles

The office and hotel buildings studied are all located in Hong Kong, which is a city with typical humid subtropical weather. The office building is located in East Kowloon, and the hotel building is in Ma Wan. Hong Kong is a coastal city located in the southern area of China and the east side of the Pearl River Estuary, and characteristics of the weather of Hong Kong are having hot, humid summers and mild, dry winters. The weather file used in this study consists of air temperature, relative humidity, wind velocity, and solar radiation from the Hong Kong Meteorological Observatory [36,37], the temperature data of seawater supported by the Hong Kong observatory, and the tidal speed data from the Hong Kong Hydrographic Office [38].

The weather analyses in terms of the solar radiation, wind velocity, and tidal stream velocity of Hong Kong according to these files are shown in Fig. 1. As shown in Fig. 1 (a), the monthly total horizontal radiation in Hong Kong varies from 63.86 kWh/m² in February to 168.50 kWh/m² in July, with an average value of 119.06 kWh/m². The wind velocity in Hong Kong shows a different seasonal trend with solar radiation; the wind in February, March, and April shows similar median velocities from 5.48 m/s to 5.54 m/s which are relatively higher among twelve months, and the wind in July shows the lowest median velocity 3.31 m/s in a year, which can be seen in Fig. 1 (b). As noticed in Fig. 1 (c), the tidal stream velocity shows similar distributions in different months during a year, the median value varies slightly from 0.74 m/s to 0.87 m/s, while the larger value occurs in March and the lower median velocity occurs in August.

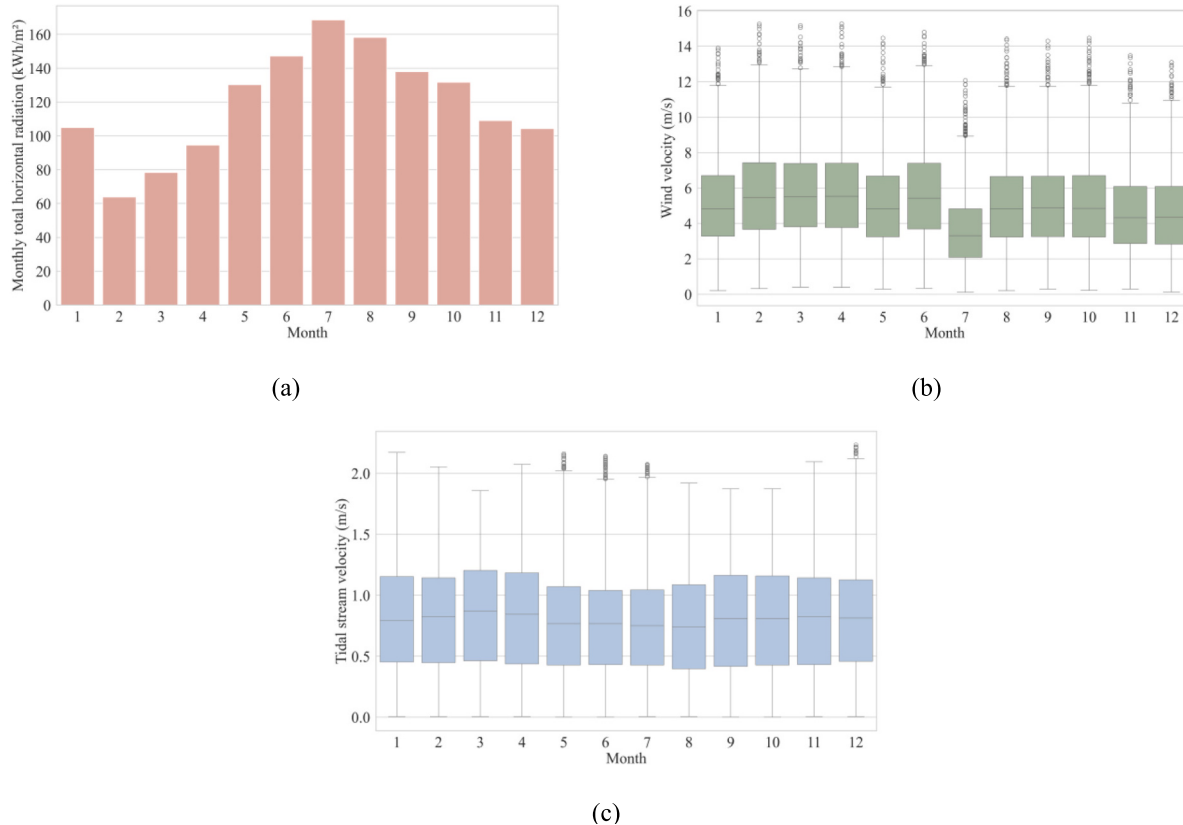


Fig. 1. Monthly weather data analysis of Hong Kong related to (a) Total horizontal radiation, (b) Wind velocity distribution, and (c) Tidal stream velocity distribution near Ma Wan.

The office building examined in this research has eleven floors, ten overground floors, and one underground floor for parking. The area for each floor is four hundred and eighty square meters and the floor height is three meters. The selection of insulation materials for envelopes and service systems of the building follows the Performance-based Building Energy Code (PB-BEC) of Hong Kong [39]. After simulation, the total annual energy demand under this condition is 1,362,081 kWh of the office building. Similarly, the hotel building studied in this research has eight floors, and the floor area and height are four hundred and eighty square meters and three meters respectively. The design of the details of the hotel building is also based on the PB-BEC of Hong Kong [39]. After simulation, the total annual energy demand of the hotel building is 883,742 kWh.

The two studied buildings belong to one hypothetical stakeholder, and the hotel building is provided for the staff working in the office building. To cover the commuting needs, 20 electric vehicles are provided to travel between these two buildings. The commute distance between the two buildings is around 25 km. The product selected for the electric vehicles is the Tesla Model S, with an 85 kWh battery capacity [40]. The daily cruise electricity consumption of EVs is calculated based on the assumption of electricity consumption to distance ratio from the study conducted by Cao [41], which is 0.13 kWh/km. The schedule for all these 20 EVs is the same. On weekdays, they are on the road from the hotel to the office from 8:00 am to 9:00 am and on the road from the office to the hotel from 6:00 pm to 7:00 pm, and all the EVs stay at the hotel at weekends. The detailed control principles and strategies for EVs are discussed in Section 3.

3. Methodology, system description, and control strategies

3.1. Simulation environment

All the simulations in this study are conducted in the software TRNSYS 18 [42] and the timestep of simulations is set as 0.25 h. TRNSYS is a powerful simulation tool for dynamic energy systems, characterized by its modular structure. Using different models, also called “Type” in the software, users can connect different thermal and electrical components and other files and functions to build a complex energy system. More importantly, users can modify and write their models to extend the ability of the software. In this study, to integrate Python language with TRNSYS to realize complicated system control strategies, the “Type

3157” component (Calling Python from TRNSYS with CFFI) written by Nicolas et al. [43] is used in TRNSYS simulations to run Python scripts. The details of the hybrid system in the simulation environment can be found in the following subsections.

3.2. The elemental system components and the basis of controls

A simplified diagram describing the hybrid system is shown in Fig. 2. The whole system mainly consists of two zero-energy buildings with integrated electric vehicles and different types of renewable energy systems. Floating PV and Offshore Wind Turbine systems are implemented beside both hotel and office buildings to utilize solar energy and wind energy. Considering the relatively higher tidal speed at Ma Wan near the hotel building, a Tidal Stream Generator system is installed to take advantage of the tidal energy there. Additional building batteries can be installed for these two buildings, respectively, as flexible energy under the developed instantaneous and predictive control mode. The two buildings are both connected to an external electricity grid. The electric vehicle integrated systems can use excessive renewable electricity power to charge EVs if the remaining renewable energy generation of the buildings is larger than the building demand after building battery processing. If there is still excessive power after charging EVs, the extra power can be exported to the external grid. Conversely, the building and the EV integrated system can also import electricity from the grid if there is an energy shortage after utilizing the energy from the building battery. Additionally, the electric vehicle integrated system also has the function of vehicle-to-building (V2B) that can be activated. This function allows EV parking inside the buildings to be discharged at a certain power to support the demand of the buildings or export extra energy to the external grid.

According to the system diagram shown in Fig. 2, several principles of controls for the hybrid system are briefly discussed. There are four kinds of control modes discussed in this study: basic control, instantaneous control, genetic predictive control for grid stability, predictive control for road impact, and grid stability. Some fundamental control principles for all these four control modes and detailed control strategies for the basic control are introduced in this section, and detailed strategies of the other three advanced control modes are introduced in Section 3.3. Considering the lower limit of the EV batteries’ FSOC level and the energy demand for commuting needs, the FSOC of EVs needs to maintain a certain level when leaving the buildings. Meanwhile, the charging

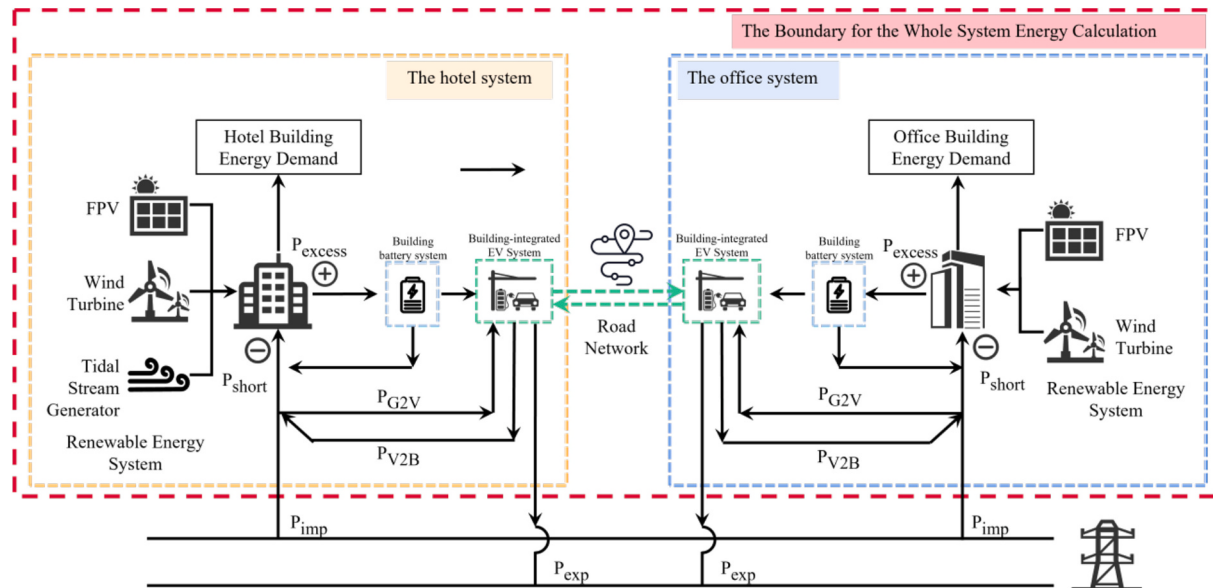


Fig. 2. System diagram of the hybrid system.

power to EVs should not let the FSOC level of EV batteries exceed the upper limit of the battery characteristic. Also, there is an upper limit of 1C for both charging and discharging power to the EV batteries. As for the detailed control strategies of the basic control mode, the V2B function is not activated in this mode, and there are no building batteries for energy flexibility. EVs are only charged when parking inside buildings. The EV-integrated system will use excessive renewable power as a priority when charging EVs. If there is no excessive renewable power and the FSOC level of EV batteries is lower than the needed value for the next travel, the building-integrated EV system will import the lowest power needed from the external grid that can charge EVs to the value at the

time leaving the building.

In the basic control mode, the energy storage capacity of EV batteries is not activated, and there are no building batteries; EVs only perform as energy consumers. To activate the energy flexibility of the whole system and to empower the building to stabilize the interaction with the grid, the V2B function of EVs is activated and building batteries are installed in the other more advanced control modes which will be discussed in Section 3.3. The V2B function can make EVs act like mobile electricity storage and share energy between the two buildings, and can also help stabilize the grid-interactive performance.

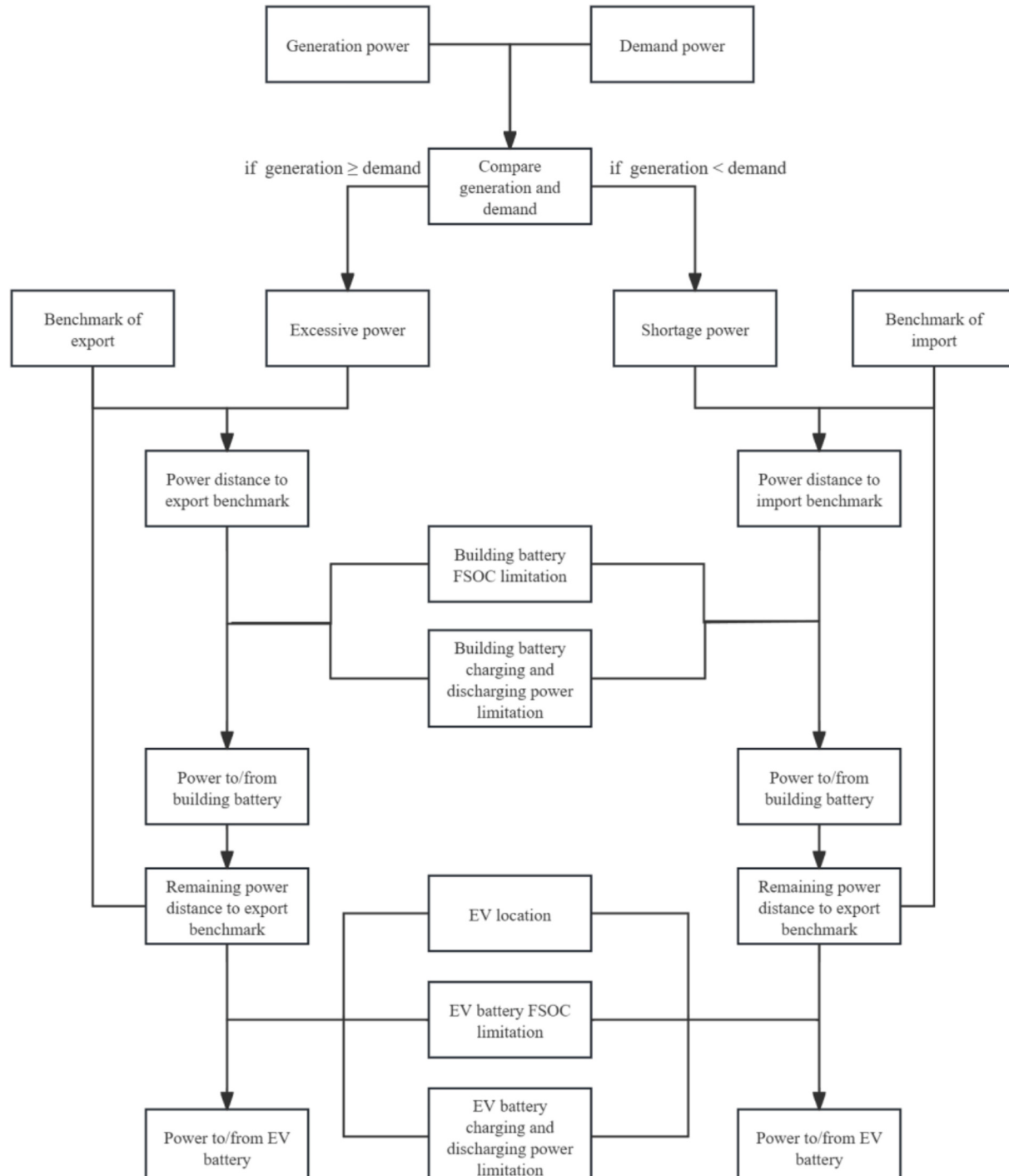


Fig. 3. Control logic of the instantaneous control.

3.3. The elaborate strategies of controls for the EV integration and sharing

3.3.1. The instantaneous control strategy with EV energy sharing by B2V and V2B

To stabilize the building-grid interaction of both the import and export side for both hotel and office buildings, four benchmarks are proposed in the instantaneous control system, which consists of the benchmark for the hotel import power from the grid ($B_{\text{hotel_imp}}$), that for the hotel export power to the grid ($B_{\text{hotel_exp}}$), and those for the office import and export power ($B_{\text{office_imp}}$, $B_{\text{office_exp}}$). In the instantaneous control system, both B2V and V2B functions of the integrated EV system in each building are activated, and building batteries are installed inside the buildings. The control objects are the charging or discharging power magnitudes of building and EV batteries. At every timestep, the objective of charging or discharging power is helping the building import or export power reach the corresponding benchmark as close as possible with certain limitations of batteries.

The detailed control logic is shown in Fig. 3. At every timestep, the power to or from the building batteries and EV batteries is utilized in the control system. These batteries have several FSOC limitations. First, the upper and lower limits on the FSOC of both building and EV batteries are assumed to be 0.95 and 0.3 in this research due to the battery characteristics. Second, if EVs are parked inside a certain building, there are additional limitations on the EV battery FSOC due to the energy requirement for the daily schedule. Considering the energy consumption at the 25 km commuting distance between the two buildings mentioned above, the lower limit on the FSOC of the EV battery when EVs are parked inside buildings is set at 0.35. Hence, there are upper charging and discharging power limits that can charge the EV battery FSOC to 0.95 or discharge it to 0.35 in one timestep (0.25 h) when EVs are parking inside a certain building, and those two limits for building

batteries are charging the FSOC to 0.95 and discharging it to 0.3 in one timestep (0.25 h), respectively. Third, in case the FSOC level of EV batteries is lower than 0.35, there is an additional lower charging power limit that can charge the batteries' FSOC level to 0.35 at the time when EVs leave the building they are parking inside. Also, there are upper charging and discharging power limits of 1C for both building and EV batteries. As mentioned above, within these charging and discharging power limits, the instantaneous control system can utilize the building batteries first and then change power to or from EVs and use them to help the import or export power of the building reach the corresponding benchmarks at each timestep if there is excessive or shortage power of the building occurring compared between renewable energy generation and energy demand at this timestep.

As for the benchmark set, the sensitivity analysis for it is discussed in Section 5, and the original benchmarks come from the simulation results under basic control. The original import power benchmark for a certain building is the average import power under the basic control mode of the time when there is a shortage of power (P_{short}) of that building, which represents that the renewable energy generation is lower than the building demand. Similarly, the original export benchmark is the average export power under the basic control mode when there is excessive power (P_{excess}) of a certain building.

3.3.2. The genetic predictive control strategy for grid stability with EV energy sharing by B2V and V2B

For the predictive control, the target is still stabilizing the building-grid interaction, and the control object is still the power to or from the building and EV batteries. The detailed control logic can be seen in Fig. 4. Within a certain prediction window, based on the predicted energy information, the instantaneous control strategy is used first to find the FSOC routes of the batteries as the input and implement a genetic

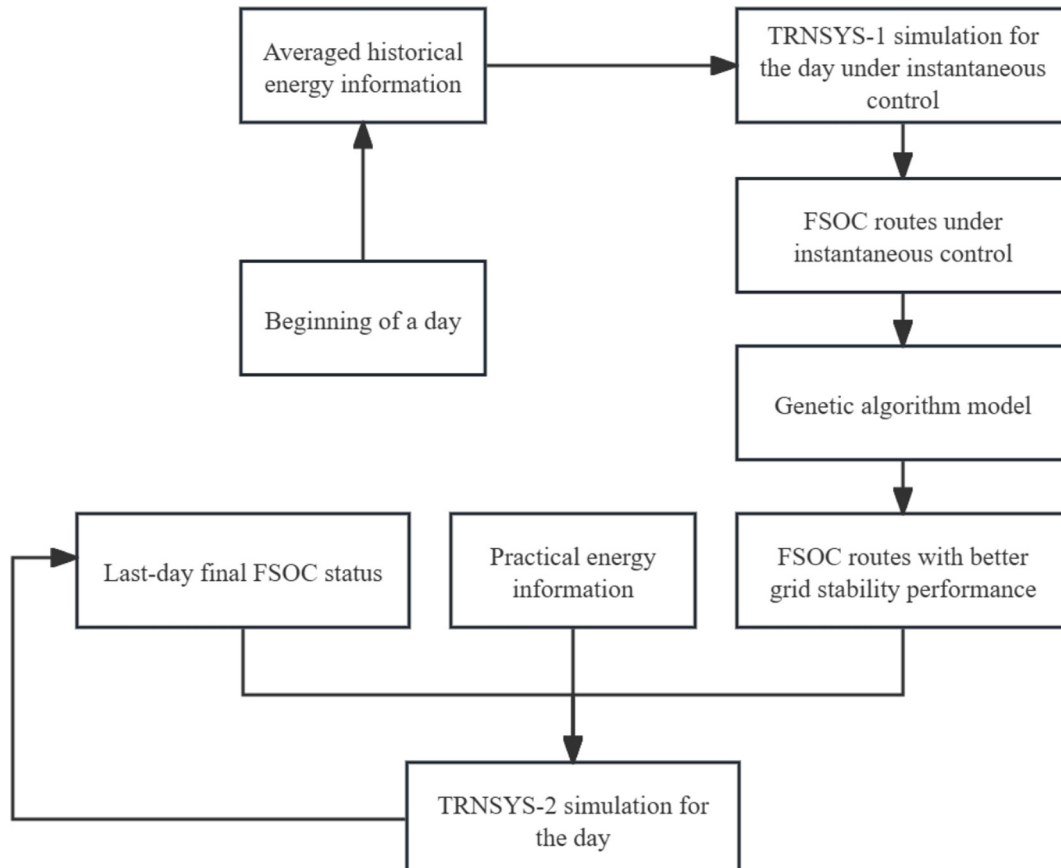


Fig. 4. Control logic of genetic predictive control for grid stability.

algorithm to find better FSOC routes than the input on the building-grid stability performance. Then the control system changes the power to or from building and EV batteries according to the FSOC routes within the prediction window. Also, the FSOC routes should be controlled within the upper and lower FSOC limits of batteries mentioned above in Section 3.3.1.

As for the prediction method, the data averaging method is implemented to get the averaged data as the predicted data based on the historical data under certain averaging levels. Through this historical data averaging approach, the data fluctuation between different years is supposed to be mitigated to improve the alignment of predicted data with practical data.

3.3.3. The predictive control strategy for road impact and grid stability with EV energy sharing by B2V and V2B

Based on genetic predictive control for grid stability, the road impact of EVs for energy sharing and commuting between two buildings is further considered in this part of predictive control. Besides the genetic control part mentioned in Section 3.3.2, additional predictive control for the road impact part is added at the beginning of each control window as shown in Fig. 5. In the road impact predictive control part, the road congestion level that will influence the time of EVs spent on the road is considered. There are twenty-five different options for EVs to leave the hotel and office. The twenty-five options vary from 7:00 am to 8:00 am from the hotel, and from 6:00 pm to 7:00 pm from the office, both with a 15-min step. At the beginning of each day, the control system will calculate the EV schedules and corresponding road impacts of every EV leaving options based on the averaged historical road congestion information, and one best schedule will be selected for the next 24 h. Then, based on the historical energy information and the EV schedule calculated with historical road information, the genetic predictive control model is implemented to find FSOC routes with better grid stability performance than instantaneous control, and the FSOC routes generated

will be used in the simulation with practical energy information and road information. In the practical simulation, the power to or from EV batteries will be adjusted according to the practical road congestion information, which will influence the practical EV schedule.

3.4. The ocean renewable energy system for buildings

3.4.1. The offshore wind energy system

Wind energy has been widely utilized in recent decades due to its clean and environmentally friendly nature. Wind turbines, a type of equipment transferring mechanical energy from wind flow to electricity, have been continuously installed over the years. The newly installed wind energy capacity was up to 117 GW in 2023 all over the world [44]. Within this 117 GW new installation, 10.8 GW was from offshore wind energy [44]. Offshore wind turbines have attracted increasing attention due to the relatively higher wind energy and lower wind shear of the site [45]. Also, the land resource usage of it is lower [45], which is especially important for a high-density city like Hong Kong.

Based on the weather analysis in Section 2 and the land scarcity of Hong Kong, offshore wind turbines are implemented beside both the hotel and office buildings to utilize wind energy. The characteristics of the product Bonus B31/300 [46,47] are used for the offshore wind turbine simulations in this paper, and the model used in TRNSYS is ‘Type 90’ in which the power-wind speed curve and other parameters such as rotor diameter and hub height can be customized to simulate the power output for different wind turbines.

3.4.2. The floating PV panel system

Solar energy is probably the most important among all renewable energy sources due to its abundant energy potential, sustainability and relatively higher efficiency, wide suitability and better affordability, and the ecosystem-friendly life cycle of solar energy utilization [48]. According to IEA, newly installed solar PV was increased to 374.9 GW in

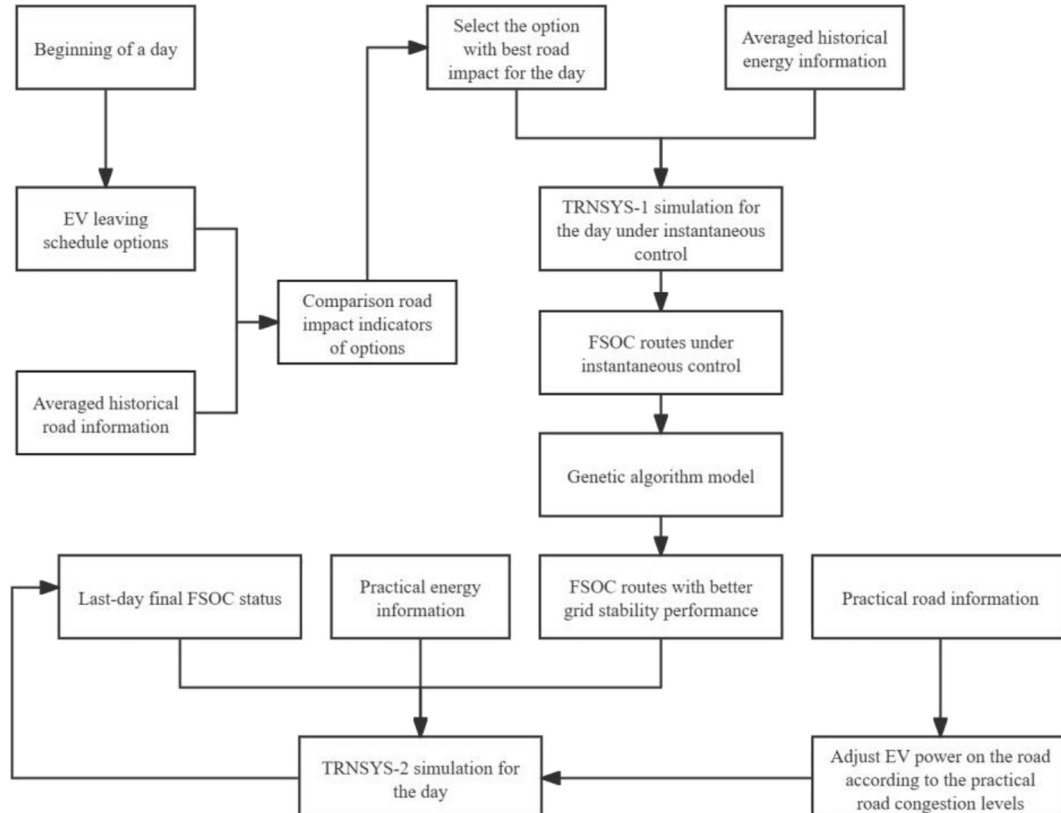


Fig. 5. Control logic of predictive control for road impact and grid stability.

2023 and accounted for around three-quarters of all the newly installed renewable energy capacity in that year [49]. Solar PV installation could be in different places like ground, rooftop, and canal tops; besides these land sites, floating PV has attracted increasing interest due to the water-cooling effect for efficiency enhancement, evaporation reduction by the PV panels, water quality protection, dust effect reduction and the contribution to the land saving [50].

The locations of the hotel and office buildings are all near the sea, and floating PV panel systems are proposed to be installed in the near-shore area beside the two buildings to exploit solar energy. There is no module in TRNSYS designed for floating PV simulations, so 'Type 567–6' is used in this paper. This module is designed for building-integrated photovoltaics (BIPV) simulations; essential settings are the back channel and back surface temperature, which can simulate the sea temperature below the floating PV system. The relatively low and stable sea temperature is important for the energy generation of the PV panels. The product FU 260 P [51] manufactured by FuturaSun is used for the characteristic inputs in the model, and several parameters at standard conditions of the product are listed in [Table 1](#).

3.4.3. The tidal stream generator

Tidal stream energy is another promising and important source of ocean energy, which comes from the rise and fall of tides caused by the gravity of the Moon, the Sun, and the Earth [52]. It is considered clean energy without pollution and has more energy potential than wave energy and ocean wind energy [53]. By implementing tidal stream generators, which have turbines working like wind turbines, the water flow of the tidal stream can be converted into electricity without using fossil fuels [54].

To utilize the tidal energy near the hotel building near Ma Wan, the tidal stream generator system is proposed to be installed. In this study, Neptune Proteus NP1000 is selected for simulation due to the accessible test data and research in past literature. There is no module in TRNSYS for TSG simulation, but the equation box can be used for the TSG output calculation based on the tidal speed. Hardisty [55] investigated the relationship between the instantaneous power output and the flow speed and implemented a generalized logistic function, which can be expressed as

$$P(t) = \frac{K}{1 + (Qe^{-B(v-M)})^{1/\gamma}} \quad (1)$$

The study also collected the test data of Neptune Proteus NP1000. Based on the data, Zhou et al. calculated the coefficients of the generalized logistic function above [56], the coefficients are listed in [Table 2](#).

3.5. Simulation groups, cases, and research steps

In this research, to thoroughly examine the impacts of renewable energy combinations and set benchmarks on the techno-economic and techno-environmental performance under basic control, developed instantaneous control and genetic predictive control, twenty-seven research groups and two additional individual cases are classified as listed in [Table 3](#). As shown in [Table 3](#), the reference case is the original system without any renewable energy system and advanced control strategy. The purpose of this case is to act as the reference for calculating the relative NPV value of the following cases with renewable energy system installation. Groups 1 to 26 contain one hundred cases each, with

Table 1

The parameters of the floating PV panel.

Module power (Pmax)	Open circuit voltage (Voc)	Short circuit current (Isc)	Maximum power voltage (Vmpp)	Maximum power current (Impp)	Module efficiency
260 W	37.59 V	8.86 A	30.65 V	8.49 A	15.92 %

Table 2

The logistic function coefficients of Neptune Proteus NP1000.

K	Q	B	M	γ
250	5.785	0.122	1.3306	0.0325

one hundred different renewable energy combinations, as shown in [Table 4](#). As the amount of TSG products is limited in the market, it is hard to assume that the TSGs with different capacities share the same characteristics. So, the number of TSGs at the hotel side in this work is based on the integer modules, and the amount has four types in the one hundred combinations, zero, two, four, and six modules. For the FPV and OWT settings in the combinations, due to the large scale of the products market, they are assumed flexible based on the percentage of the system demand they need to cover, and the left part after implementing integer modules of FPV and OWT is assumed to be covered by smaller size products of them that share the same characteristics with the original modules. The capacity types of OWT of the office side are set as 100 %, 75 %, 50 %, 25 %, and 0 % of the office demand. Simultaneously, the capacity types of FPV on the office side are set as 0 %, 25 %, 50 %, 75 %, and 100 % of the office demand. Thus, there are five combinations of office OWT and FPV systems. Similarly, there are also these five combinations of hotel OWT and FPV systems that cover the rest of hotel demand uncovered by the hotel TSG system. The cases in Group 1 are under basic traditional control, and cases in Group 2 are under the developed instantaneous control with original benchmarks. The cases in Groups 3 to 26 are under instantaneous control with changed import or/and export benchmarks from -100 % to 100 % with a 25 % step compared to original benchmarks. The case for predictive control development is the representative case from Groups 2 to 26 with a change from instantaneous control to predictive control. The cases in Group 27 are similar to those in the benchmark group which the representative case is in and are just with a change from instantaneous control to predictive control. As for the cases in Group 28, three representative renewable energy combinations will be selected for simulation, and the benchmarks are the same as those of Group 27. The control in Group 28 is changed to predictive control for road impact and grid stability.

The illustration of the research steps of this study is demonstrated in [Fig. 6](#). First, the reference case is simulated as the calculation base for the relative net present value. Second, cases in Group 1 under basic control are simulated to calculate the benchmarks for instantaneous control. Third, cases in Group 2 under instantaneous control with original benchmarks are analyzed to investigate the impact of renewable energy systems on the system performance, with detailed analysis provided in [Section 5.1](#). Fourth, cases in Groups 3 to 26 with the benchmarks changed according to the rules mentioned above are analyzed to study the impact of benchmarks on the system performance under instantaneous control, and the analysis is also conducted in [Section 5.1](#) in detail. Five, a representative case from [Section 5.1](#) is selected for methodology development of the predictive control in [Section 5.2](#). Six, based on the developed predictive control algorithm, cases in Group 27 with different renewable energy system combinations are simulated to investigate the impact of different renewable energy types on the system performance and enhancement of predictive control. Lastly, cases under predictive control for road impact and grid stability with three representative renewable combinations are simulated in Group 28 to investigate the road impact enhancement of control 3 and the corresponding influence on grid-interaction stability performance.

4. Analysis criteria

To evaluate the performance of the simulated system of different criteria under various controls, some indicators are implemented in this study. The performance of the system is evaluated from four aspects: energy, economic, environmental, and traffic aspects. Within the energy

Table 3

Simulation groups and cases.

Group/case No.	Renewable energy system combinations					Control algorithm	Change of import benchmark	Change of export benchmark
	Hotel OWT *	Hotel FPV *	Hotel TSG (modules)	Office OWT	Office FPV			
Reference	NA	NA	NA	NA	NA	Basic control	NA	NA
1	100 %, 75 %, 50 %, 25 %, 0 %	0 %, 25 %, 50 %, 75 %, 100 %	0, 2, 4, 6	100 %, 75 %, 50 %, 25 %, 0 %	0 %, 25 %, 50 %, 75 %, 100 %	Basic control	NA	NA
2-26	100 %, 75 %, 50 %, 25 %, 0 %	0 %, 25 %, 50 %, 75 %, 100 %	0, 2, 4, 6	100 %, 75 %, 50 %, 25 %, 0 %	0 %, 25 %, 50 %, 75 %, 100 %	Control 1**	0 % -100 % to +100 % with a 25 % step	-100 % to +100 % with a 25 % step 0 %
Representative	Representative combination (combination 38)					Basic control and control 1 & 2	Representative benchmark group (group 8)	
27	100 %, 75 %, 50 %, 25 %, 0 %	0 %, 25 %, 50 %, 75 %, 100 %	0, 2, 4, 6	100 %, 75 %, 50 %, 25 %, 0 %	0 %, 25 %, 50 %, 75 %, 100 %	Control 2**	Representative benchmark group (group 8)	
28	Three representative combinations (combination 14, 29 38)					Control 3**	Representative benchmark group (group 8)	

*: The percentage of OWT and FPV of the hotel is for the rest demand after TSG system implementation.

**: Control 1: instantaneous control; Control 2: genetic predictive control for grid stability; Control 3: predictive control for road impact and grid stability.

Table 4

Renewable energy type combinations.

Combination No.	Hotel OWT (% of hotel rest demand after TSG)	Hotel FPV (% of hotel rest demand after TSG)	Hotel TSG (modules)	Office OWT (% of office demand)	Office FPV (% of office demand)
1-5	100	0	0	100-0 (step25)	0-100 (step25)
6-10	75	25	0	100-0 (step25)	0-100 (step25)
11-15	50	50	0	100-0 (step25)	0-100 (step25)
16-20	25	75	0	100-0 (step25)	0-100 (step25)
21-25	0	100	0	100-0 (step25)	0-100 (step25)
26-30	100	0	2	100-0 (step25)	0-100 (step25)
31-35	75	25	2	100-0 (step25)	0-100 (step25)
36-40	50	50	2	100-0 (step25)	0-100 (step25)
41-45	25	75	2	100-0 (step25)	0-100 (step25)
46-50	0	100	2	100-0 (step25)	0-100 (step25)
51-55	100	0	4	100-0 (step25)	0-100 (step25)
56-60	75	25	4	100-0 (step25)	0-100 (step25)
61-65	50	50	4	100-0 (step25)	0-100 (step25)
66-70	25	75	4	100-0 (step25)	0-100 (step25)
71-75	0	100	4	100-0 (step25)	0-100 (step25)
76-80	100	0	6	100-0 (step25)	0-100 (step25)
81-85	75	25	6	100-0 (step25)	0-100 (step25)
86-90	50	50	6	100-0 (step25)	0-100 (step25)
91-95	25	75	6	100-0 (step25)	0-100 (step25)
96-100	0	100	6	100-0 (step25)	0-100 (step25)

aspect, both grid interaction stability and system energy-matching performances are considered.

For energy aspect evaluation, annual grid interaction stability for imported and exported power of both hotel and office buildings are evaluated using four standard deviation indicators respectively, the four indicators (σ_{imp_hotel} , σ_{exp_hotel} , σ_{imp_office} , σ_{exp_office}) are calculated based on the four equations from (2) to (5). In these equations, n is the number of timesteps in the annual simulation that the corresponding imported or exported power is larger than zero.

$$\sigma_{imp_hotel} = \sqrt{\frac{\sum_{i=1}^n (P_{imp_hotel,i} - \bar{P}_{imp_hotel})^2}{n}} \quad (2)$$

$$\sigma_{exp_hotel} = \sqrt{\frac{\sum_{i=1}^n (P_{exp_hotel,i} - \bar{P}_{exp_hotel})^2}{n}} \quad (3)$$

$$\sigma_{imp_office} = \sqrt{\frac{\sum_{i=1}^n (P_{imp_office,i} - \bar{P}_{imp_office})^2}{n}} \quad (4)$$

$$\sigma_{exp_office} = \sqrt{\frac{\sum_{i=1}^n (P_{exp_office,i} - \bar{P}_{exp_office})^2}{n}} \quad (5)$$

To compare the overall grid stability performances of the system among different simulation cases, a normalized weighted stability indicator (WSI) is introduced. The equation is as shown in Eq. (6): the WSI is between 0 and 1, and the larger the WSI, the more stable the grid interaction of the system is.

$$WSI = w_1 \times \left(1 - \frac{\sigma_{imp_hotel}}{\sigma_{imp_hotel_max}}\right) + w_2 \times \left(1 - \frac{\sigma_{exp_hotel}}{\sigma_{exp_hotel_max}}\right) + w_3 \times \left(1 - \frac{\sigma_{imp_office}}{\sigma_{imp_office_max}}\right) + w_4 \times \left(1 - \frac{\sigma_{exp_office}}{\sigma_{exp_office_max}}\right), 0 \leq WSI \leq 1 \quad (6)$$

In this study, the four grid stability indicators are considered to have the same priority in the system's overall grid stability evaluation, so the four weighted factors w_1 to w_4 are set as the same value of 0.25.

Energy matching is another important performance of the system that needs to be evaluated. In this research, on-site electrical energy matching, on-site electrical energy fraction, and weighted matching index combined with them, extracted from Cao et al. [57] and abbreviated as OEMe, OEEFe, and WMI, respectively, are utilized to evaluate

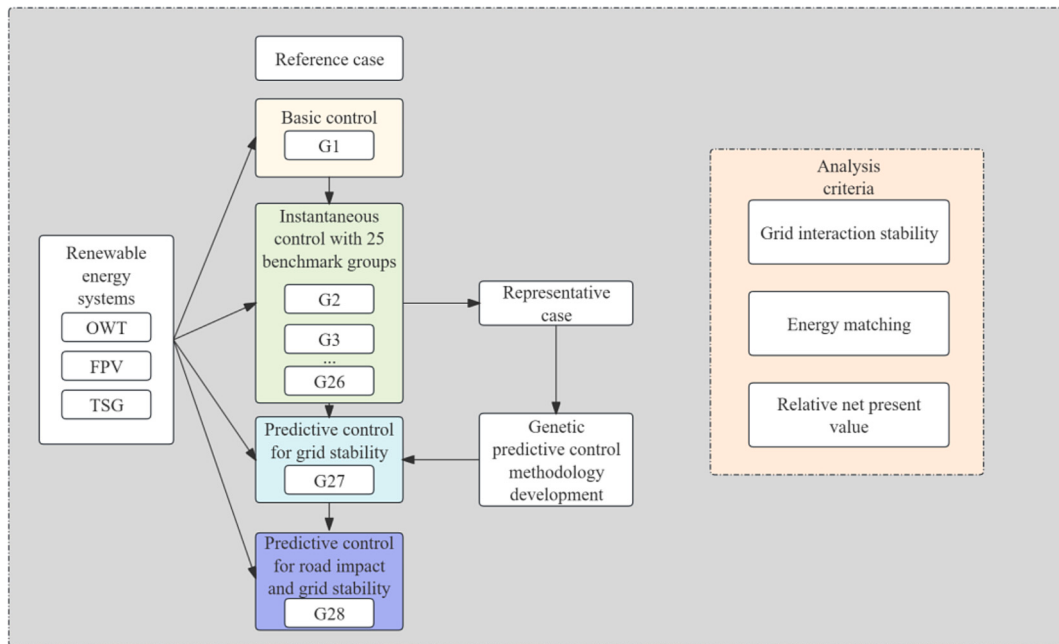


Fig. 6. Research steps and analysis criteria.

the proportion of renewable energy being used on-site within the building and the fraction of the demand being covered by renewable energy. The three indicators are calculated based on the equations from (7) to (9).

$$\text{OFE}_e = 1 - \frac{\int_{t_1}^{t_2} P_{imp,sys}(t) dt}{\int_{t_1}^{t_2} [L_{elec,sys}(t) + P_{EV,sys}(t)] dt}, 0 \leq \text{OFE}_e \leq 1 \quad (7)$$

$$\text{OME}_e = 1 - \frac{\int_{t_1}^{t_2} P_{exp,sys}(t) dt}{\int_{t_1}^{t_2} P_{RE,sys}(t) dt}, 0 \leq \text{OME}_e \leq 1 \quad (8)$$

$$\text{WMI} = w_1 \times \text{OFE}_e + w_2 \times \text{OME}_e, 0 \leq \text{WMI} \leq 1 \quad (9)$$

Similar to WSI, in this study, the OFE_e and OEM_e are considered to share the same importance in the final assessment of energy-matching performance, w_1 and w_2 are both set as 0.5 in Eq. (9).

For the economic aspect, the 20-year relative net present value compared with the original system under basic control and without any renewable energy system implementation. The calculation equation for the relative NPV (NPV_{rel}) is as below. In the equation, C_{REE} Is the Feed-in Tariff [58] income for the electricity generation from renewable energy, $C_{imp,save}$ is the bill reduction because of the saved imported energy, C_{sv} is the salvage value of the batteries, $C_{O\&M}$ and C_{repl} are the operation and maintenance fees and replacement costs of the system respectively. I_{REE} is the initial investment for the renewable energy system installation, n is the number of years the system has been operating, and i is the real interest rate. As shown in Table 5, i is set as 2.75 % in this study according to the average real interest rate of the recent 10 years from 2014 to 2023 of Hong Kong SAR provided by The World Bank Group [59]. Other tariff model settings and the cost of the hybrid system are also specified in Table 5 for calculating different parameters in the equation.

First, investment, operational, and maintenance fees of different renewable energy systems need to be considered in this study, the initial investment of offshore wind turbines is set as 29,526 HKD/kW, and operational and maintenance (O&M) is set as 0.92 % of the initial cost every year [47,60]. Those of floating PV and TSG systems are set as 26,520 HKD/kW and 1.92 %, 19,110 HKD/kW and 5 %, respectively [56,60,61]. Second, according to Hsieh et al. [62], the replacement cost of EV batteries is set as 1566 HKD/kWh, and the battery degradation model is set as a simple cycle number-based model, the maximum cycle number is set as 2000 with a maximum lifetime of 8 years. In this study, building batteries are considered to share the same economic settings with the EV batteries. Third, the cost of the electricity imported is set as a simple constant tariff model of 1.544 HKD/kWh from CLP [63], one of the main electricity power generation companies in Hong Kong. Last, the stakeholder can benefit from the generated renewable energy according to the Feed-in Tariff by the Hong Kong government from 2.5 to 4 HKD per kWh with respect to different system-generating capacities [58].

$$NPV_{rel} = \sum_{n=1}^{20} \left(\frac{C_{REE,n} + C_{imp,save,n} + C_{sv} - C_{O\&M,n} - C_{repl,n}}{(1+i)^n} \right) - I_{REE} \quad (10)$$

For the environmental aspect, the annual net imported energy of the whole system from the external grid and the corresponding annual net equivalent carbon emission (CE_a) are calculated using the equations below for the environmental impact evaluation. In Eq. (12), CEF_{eg} is the equivalent carbon dioxide emission factor of the electrical energy imported from the grid. According to the sustainability report of CLP, the CEF_{eg} is set as 0.55 kg CO₂, eq/kWh in this study [64].

$$E_{direct,sys} = \int_{t_1}^{t_2} P_{imp,sys}(t) dt - \int_{t_1}^{t_2} P_{exp,sys}(t) dt \quad (11)$$

Table 5
Parameters for the cost and income calculations of the hybrid system.

	Offshore Wind Turbine	Floating PV	Tidal Stream Generator	EV battery / Building battery	Electricity tariff	Feed-in Tariff	Interest rate
Initial investment O&M	29,526 HKD/kW 0.92 %	26,520 HKD/kW 1.92 %	19,110 HKD/kW 5 %	1566 HKD/kWh (Replacement time 8 years)	1.544 HKD/kWh	2.5–4 HKD/kWh	2.75 %

$$CE_a = E_{direct,sys} \times CEF_{eg} \quad (12)$$

For the traffic aspect evaluation, the annual positive, negative, and overall impact (PRI, NRI, and ORI) of commuting EVs on the road between two buildings are calculated for every case. The road is divided into 5 sections in this study. According to road data from Google Maps, each section has a congestion signal from 1 to 4 every 15 min, where 1 means the section of the road is completely non-congested and 4 means the section is in heavy congestion condition. The road impact calculation will be based on these signals and using the following equations:

$$PRI = \frac{\sum_{j=1}^D n_j}{m \cdot D} \cdot \frac{\sum_{j=1}^D (\sum_{i=1}^m T_{min,i} \cdot F_{min})_j}{\sum_{j=1}^D (\sum_{i=1}^m T_i \cdot F_i)_j}, F_i < 2.5, 0 \leq PRI \leq 1 \quad (13)$$

$$NRI = \frac{\sum_{j=1}^D n_j}{m \cdot D} \cdot \frac{\sum_{j=1}^D (\sum_{i=1}^m T_i \cdot F_i)_j}{\sum_{j=1}^D (\sum_{i=1}^m T_{max,i} \cdot F_{max})_j}, F_i \geq 2.5, 0 \leq NRI \leq 1 \quad (14)$$

$$ORI = PRI - NRI, -1 \leq ORI \leq 1 \quad (15)$$

In Eqs. (13) and (14), F_i is the congestion signal of the section i and T_i is the corresponding time needed to travel through this section, n_j is the number of sections where the congestion signal is lower or larger than 2.5 respectively in the day j , D is the number of days that EVs need to commute between two buildings, and m is the number of sections of the road in two directions.

5. The results, analyses, and discussions of simulations

As discussed in Section 3.5, besides the reference and representative cases, the cases in this study are divided into twenty-eight groups, which can be seen in Table 3. The reference case is without renewable energy penetration and corresponding control strategies. There are one hundred cases in each group within Group 1 to Group 26 with one hundred renewable energy combinations. The control strategy of Group 1 is basic control and that of Groups 2 to 26 is the developed instantaneous control. The variables among Groups 2 to 26 are the setting of control benchmarks for grid stability. After analyzing the cases under instantaneous control, a representative case from Groups 2 to 26 with relatively better performance is selected for the development of predictive control. After the development of predictive control, the cases in Group 27 simulate the performance of predictive control under different renewable energy combinations. In Group 28, the control is changed to predictive control for road impact and grid stability and implemented on three representative renewable energy combinations. The research steps are discussed in Section 3.5 and the diagram can be seen in Fig. 6. The twenty-eight case groups together with reference and representative cases are simulated in TRNSYS 18 and analyzed in three criteria. The results of the simulations are presented and analyzed in this section. As mentioned in Section 3.5, Section 5.1 discusses the impact of different renewable energy combinations on the system performance and presents the techno-economic analysis of various control benchmarks for grid stability in the instantaneous control. Section 5.2 shows the development of the genetic predictive control for grid stability for the representative case from Section 5.1. Section 5.3 investigates the impact of renewable energy combinations under predictive control. Finally, Section 5.4 presents and analyzes the results of cases with predictive control for road impact and grid stability.

5.1. Instantaneous control: The impact of ocean renewable energy systems and the benchmarks

Two variables, ocean renewable energy systems and benchmarks, affect the system performance under instantaneous control in this study. As mentioned above, two thousand and five hundred cases with one hundred types of renewable energy combinations and 25 types of

benchmark combinations are simulated and analyzed under instantaneous control. The techno-economic performance of different cases is evaluated based on the indicators mentioned in Section 4.

- (1) The impact of the ocean renewable energy systems on techno-economic performance

One hundred cases in Group 2 under instantaneous control with original benchmarks are analyzed in this sub-section. Each case has different proportions of OWT, FPV, and TSG systems for the system as illustrated in Table 3.

First, the impact of OWT and FPV systems is investigated in cases without TSG. Fig. 7 shows the performance of these cases on grid stability, energy matching, and economic benefit. As shown in Fig. 7 (a), the case with 100 % FPV systems has a higher WSI than the case with 100 % OWT systems (0.580 vs 0.459), which indicates the higher stability of 100 % solar energy than 100 % wind energy in this hybrid system due to the characteristic that the majority of the system demand happens in the daytime, aligning with the solar energy characteristic. Introducing 100 % OWT penetration into the system may bring extra fluctuation at nighttime. Moreover, mixed systems with 50 %:50 % to 25 %:75 % of wind and solar energy have better stability performance under instantaneous control. A system with 50 % and 25 % wind energy, 50 % and 75 % solar energy for the office and hotel, respectively, has the best performance on stability, with a WSI of 0.643, which indicates that introducing appropriate wind energy into the system to cover the night demand can make the system more stable under instantaneous control. Similar trends can also be noticed in the energy matching in Fig. 7 (b). The system fully relying on FPV shows a better WMI than 100 % OWT, and mixed utilization of solar and wind energy can also bring better energy-matching performance than a single energy type. The peak energy-matching comes from the case with 25 % OWT 75 % FPV for the office and 50 % OWT 50 % FPV for the hotel, of which the WMI is 0.577. The reason may be the higher proportion of daytime demand of the office than the hotel, which is better matched with higher solar energy penetration. As illustrated in Fig. 7 (c), by increasing the proportion of the FPV system, the NPV_{rel} of this system would be decreased, which means that OWT shows better economic benefits on a 20-year scale than FPV. 100 % penetration of OWT has a 31.639 million HKD higher NPV_{rel} than the case with 100 % FPV.

Second, for analyzing the impact of TSG on the system performance, the cases with four types of TSG modules at the hotel side are simulated and presented in Fig. 8, where the remaining demand is supported fully by OWT or FPV. Each TSG module can support around 15.8 % of the hotel demand. As shown in Fig. 8 (a), when considering TSG and OWT only, introducing tidal energy will first increase the grid stability and then decrease it. The case with two TSG modules shows the best WSI of 0.493 among the four cases. The same trend is noticed when considering TSG and FPV. Introducing TSG will also improve energy-matching first and then decrease it. 63.2 % penetration of tidal energy with six TSG modules at the hotel show higher energy-matching performances with WMI of 0.438 and 0.528 respectively. These two trends show that introducing appropriate penetration of tidal energy can benefit both grid stability and energy-matching performance in this kind of coastal building system. As shown in Fig. 8 (c), TSG shows poorer economic performance than OWT and FPV. Among the cases just with TSG and OWT, the case with six modules of TSGs and supplemented by OWT has a 32.956 million HKD poorer NPV_{rel} than the case with 100 % OWT. When considering TSG and FPV, the case with six modules of TSGs shows 17.766 million HKD poorer NPV_{rel} than the case with 100 % FPV.

Taking the grid stability, energy matching, and economic benefits into account, one hundred cases with different renewable energy combinations in Group 2 are plotted in Fig. 9. Fourteen cases on the Pareto front are plotted in colored dots. Among fourteen combinations, combination 38 is selected as the representative combination for the following analyses. The combination is almost equally distributed for

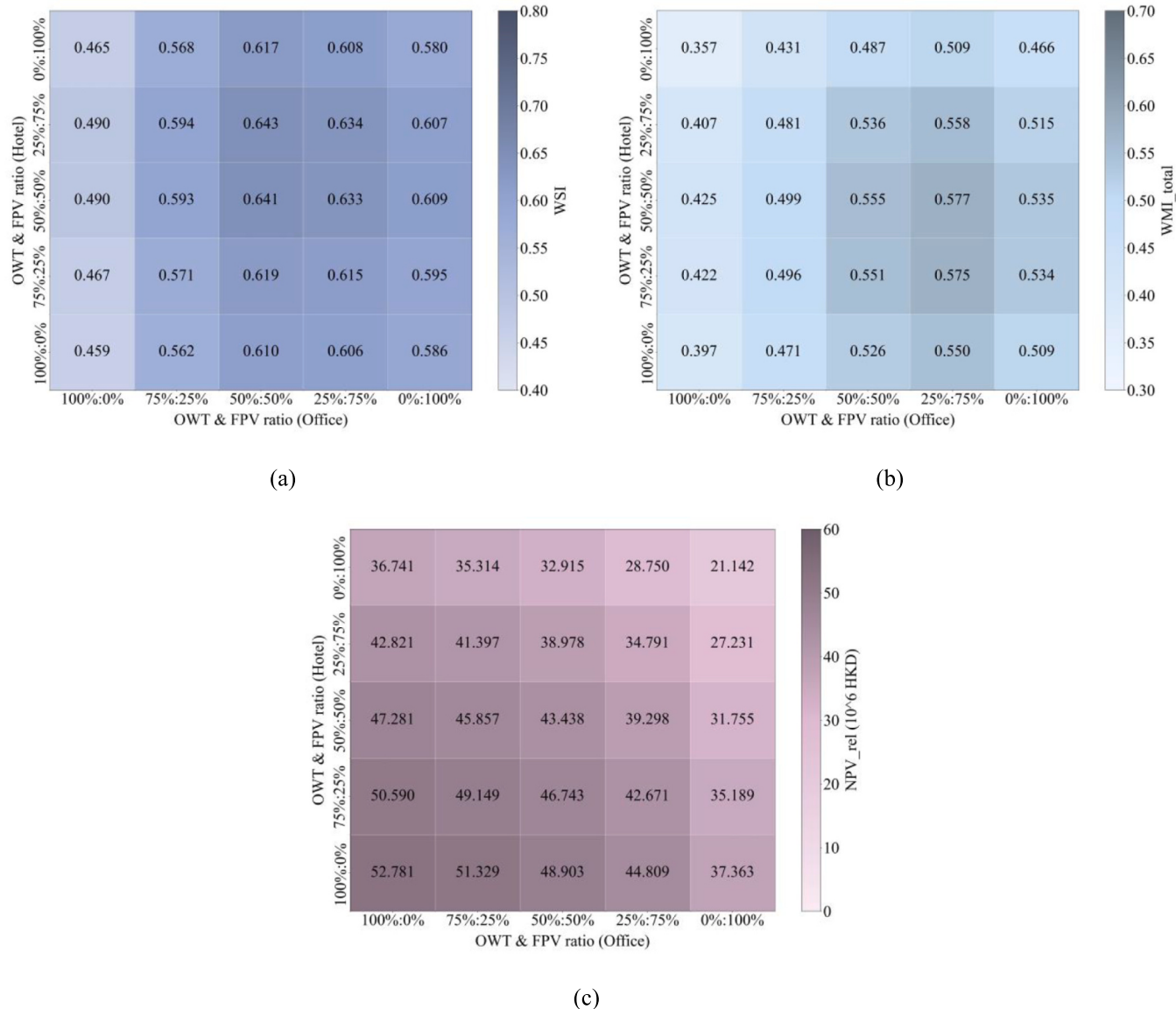


Fig. 7. System performance of cases in Group 2 with different proportions of OWT and FPV regarding (a) Grid-interaction stability, (b) Energy matching, and (c) Relative net present value.

the three types of renewable energy systems. It consists of two TSG modules the hotel and the remaining system demand is covered by OWT and FPV in a 50 %:50 % ratio. The case with combination 38 in Group 2 has a WSI of 0.659, a WMI of 0.578, and a NPV_{rel} of 35.837 million HKD.

(2) The impact of the benchmarks of the instantaneous control on technical and economic performance

Twenty-five groups of cases are simulated under instantaneous control with different benchmarks mentioned in Table 3. In each group, the case with combination 38, which is on the Pareto front in Fig. 9, is selected for the benchmark analysis. The system performance of these twenty-five cases in grid stability, energy matching, and economic benefit are analyzed and plotted in Fig. 10 respectively. The energy performance of case G1C38 with combination 38 under basic control is calculated to compare with instantaneous control. The WSI and WMI of it are 0.410 and 0.618, respectively.

As shown in Fig. 10 (a), when the import benchmark remains original, a -25% change in the export benchmark shows the best grid stability of 0.662. When the export benchmark remains the original, the

most effective import benchmark is with a change of $+25\%$. Among all the twenty-five groups, the most effective benchmark group is that with changes of $+50\%$ on both import and export benchmarks, and the WSI is 0.701. In all three scenarios mentioned above, both decrease and increase on the most effective benchmarks would cause poorer grid stability. It is noticed that the original benchmarks are quite effective and have a 60.7 % improvement of WSI from 0.410 to 0.659. As for the energy-matching, the trend is clear as illustrated in Fig. 10 (b): the performance is improved with decreased import and export benchmarks. The reason is that lower control benchmarks mean a more matching-based control, the system tries to import and export less energy from and to the grid. The case under fully matching-based control with -100% benchmarks has a WMI of 0.751, 21.5 % higher than that of the system under basic control. However, this fully matching-based control will result in a 9.3 % reduction in WSI from 0.410 to 0.372 compared with basic control. The impact of benchmarks on the economic benefits shown in Fig. 10 (c) is similar to that on energy matching. Lower import and export benchmarks mean less imported energy from the grid and more saved cost compared to the reference case. Simultaneously, as the FiT subsidies are based on the renewable energy

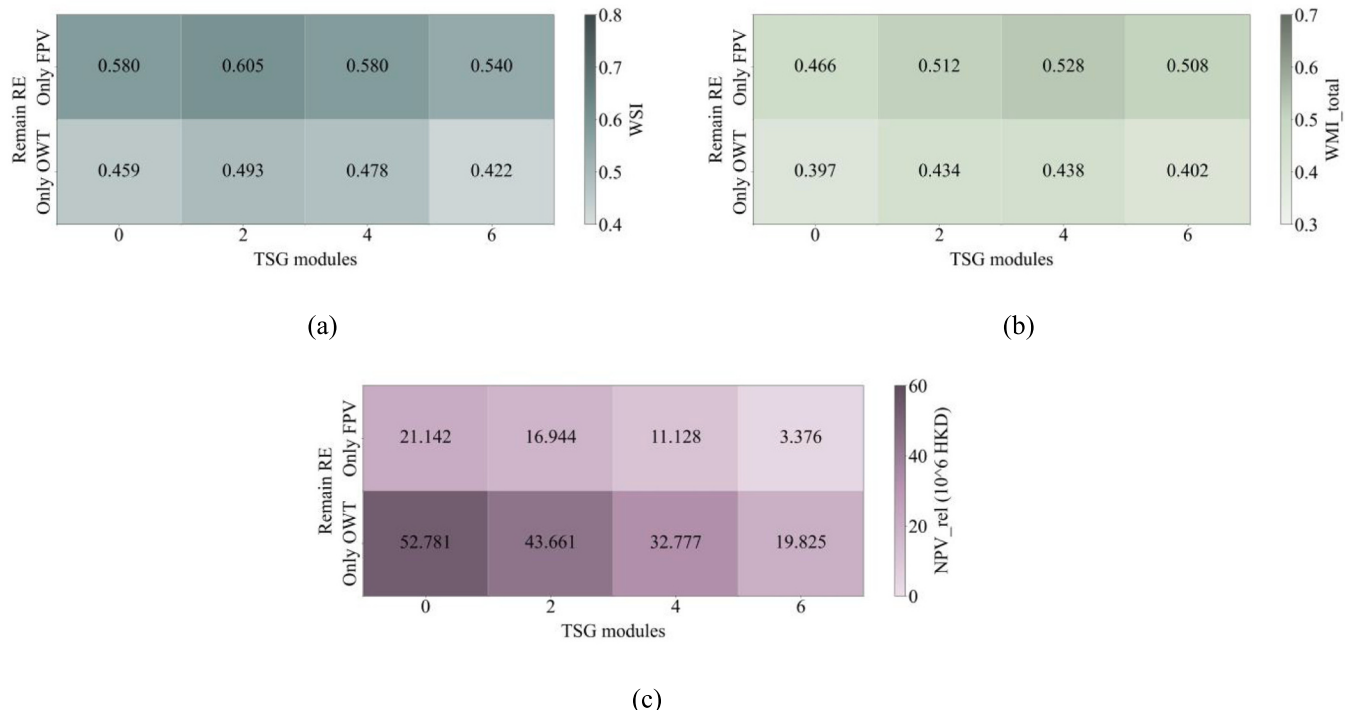


Fig. 8. System performance of cases in Group 2 with the implementation of TSG regarding (a) Grid-interaction stability, (b) Energy matching, and (c) Relative net present value.

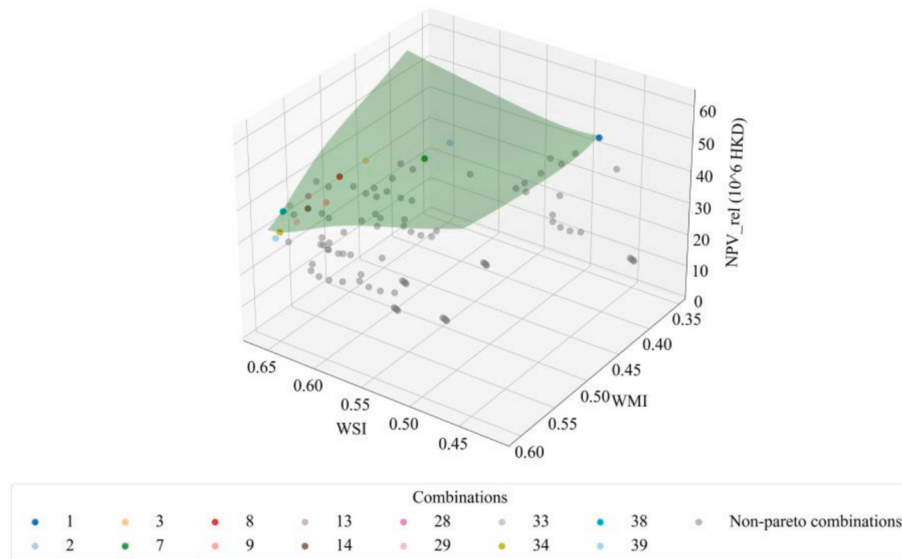


Fig. 9. Pareto front of the one hundred combinations in Group 2.

produced other than exported, lower benchmarks would not affect this income. These result in that the system's performance on economic benefits is in line with the performance on energy matching.

As shown in Fig. 11, Ten benchmark groups are on the Pareto front based on grid stability, energy matching, and economic benefits. Within ten cases, the case in group 8 (case G8C38) is selected as the representative case for instantaneous control, which has the original import benchmark and a – 50 % change in the export benchmark. The NPV_{rel} of it is 38.273 million HKD and the CE_a is 682.774 kg. The comparison on grid-interaction stability and energy matching between this case and the corresponding case under basic control can be seen in Fig. 12. With instantaneous control for grid stability, the WSI of the system is

improved from 0.410 to 0.644 by 57.1 % while the energy-matching indicator WMI remains almost at the same level, with a slight increase from 0.618 to 0.625 by 1.1 %.

Based on the abovementioned analyses presented in this subsection, for the coastal ZEBs system supported by ocean renewable energy discussed in this study, solely introducing solar energy shows a better technical performance than solely introducing wind energy. However, hybrid systems with multiple types of renewable energy provide higher stability and matching performance than individual systems. The recommended penetration ratio is 50 %:50 % to 25 %:75 % for offshore wind and solar energy generation systems. In terms of economic performance, OWT shows the best performance and FPV is better than TSG

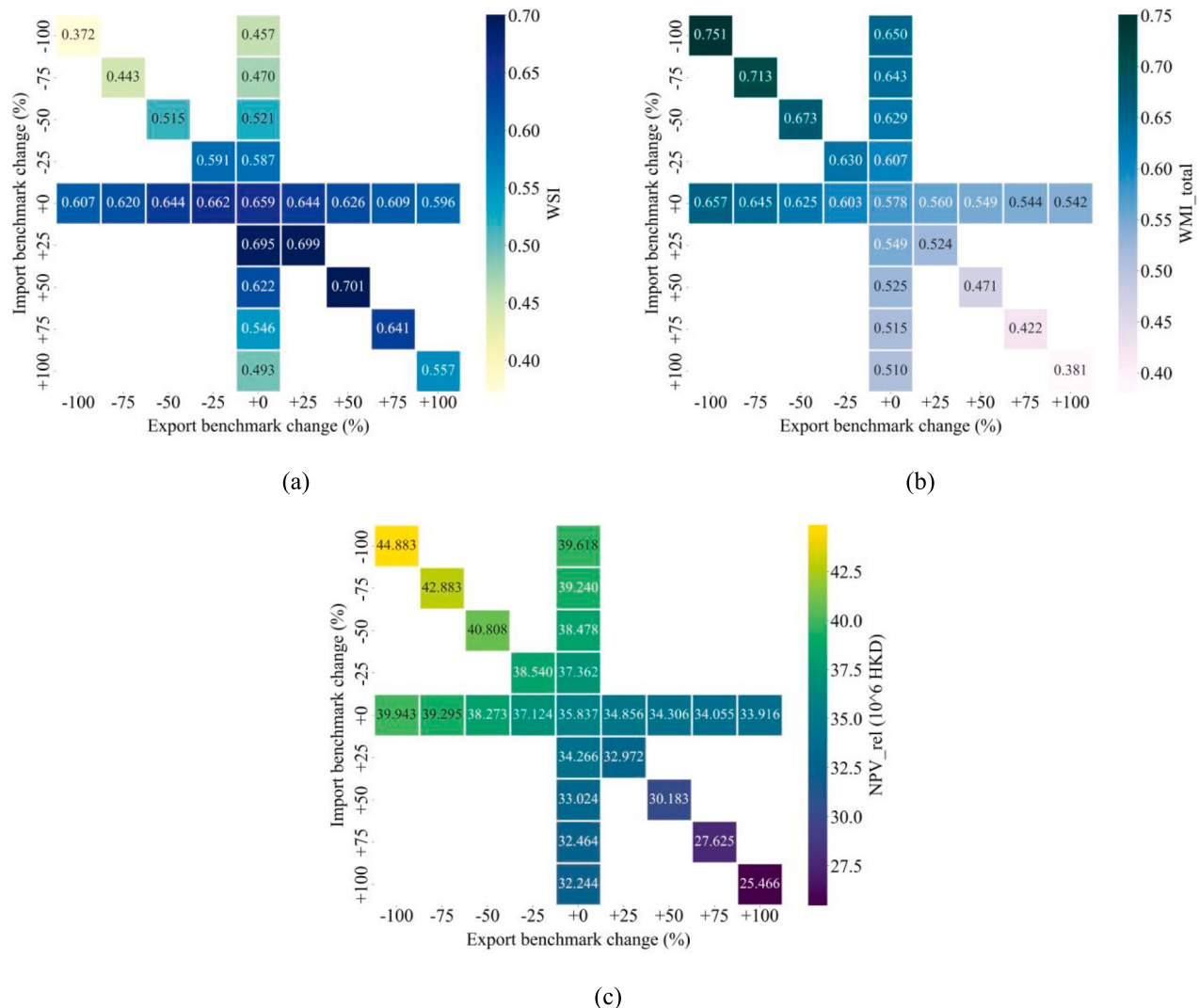


Fig. 10. System performance of cases with different benchmarks under instantaneous control regarding (a) Grid-interaction stability, (b) Energy matching, and (c) Relative net present value.

systems. When introducing tidal stream energy to ZEBs like hotels that have relatively equally distributed daytime and nighttime demand, it is recommended to cover around 30 % of building demand to get better energy performance and acceptable economic sacrifice. As for the implementation of the developed instantaneous control approach for stabilizing the grid interaction, the recommended change ratio added on the original import and export benchmarks calculated by the method presented in Section 3.3.1 is from -50 % to +50 %, depending on the focus of the control determined by stakeholders is more on grid stability or on energy-matching, which can at least provide a 25.6 % enhancement on the WSI in the presented cases.

5.2. Methodology development of genetic predictive control for grid stability

Based on the analyses above, instantaneous control has been proven to be quite effective in stabilizing the grid-interactive performance. However, the instantaneous control is according to the energy information of the current moment, and the batteries may lose flexibility for future timesteps. Integrating the short-term predicted energy information into the control process of the current timestep is proposed to enable the system to have a more stable grid interactive performance on an annual scale.

The energy information used for predictive control is the electricity demand of two buildings and the electricity generation of renewable energy systems. There are two datasets in the predictive control simulation: historical data and practical data. In this preliminary study, the electricity generation of renewable energy systems is assumed to be the same between the two datasets. As for the building demand, the building demand mentioned in Section 2 is set as the historical demand data. To get the practical demand data, deviation factors from -10 % to 10 % that follow a normal distribution are given to the building demand of every time step. After processing, the new dataset is set as the practical demand data for simulation under predictive control.

The predictive control method is shown in Fig. 4. The control window is set as twenty-four hours, and at the beginning of every control window, the averaged historical building demand is proposed to be predicted data and would be put in the first TRNSYS to simulate the energy flow under instantaneous control. In this work, the average level of historical data is set as 0.25 h. After simulation, three FSOC routes of two building batteries and EV batteries of that control window would be used as initial inputs for the genetic algorithm model. Within the genetic model, each individual contains the three routes of three batteries, and each population contains fifty individuals. The generation number of each round of genetic algorithm operation is set as 6000 to find better routes that can make the buildings' imported and exported power closer

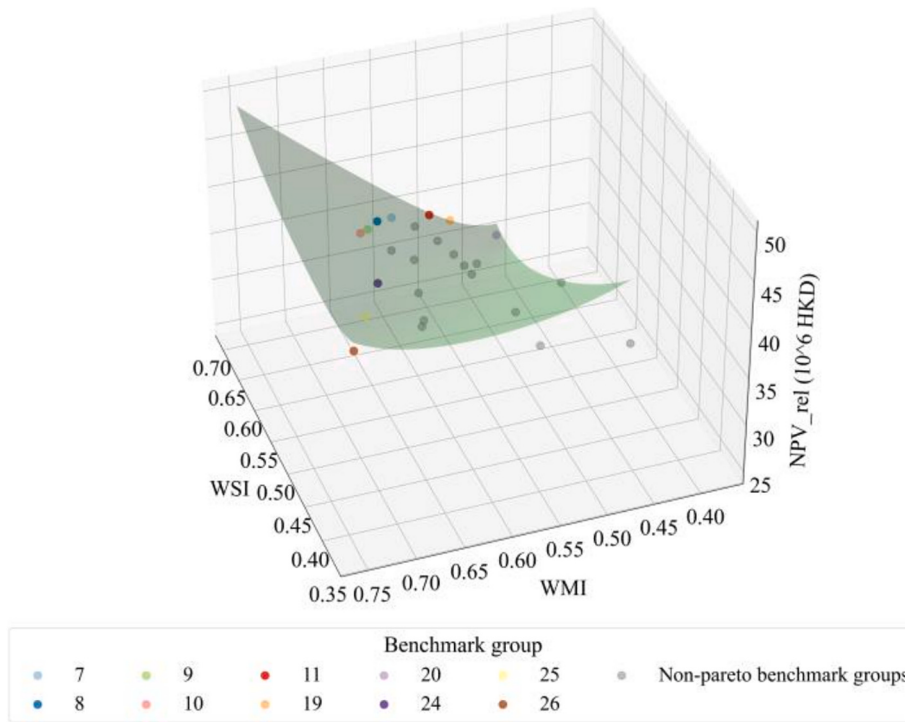


Fig. 11. Pareto front of cases with different benchmarks under instantaneous control.

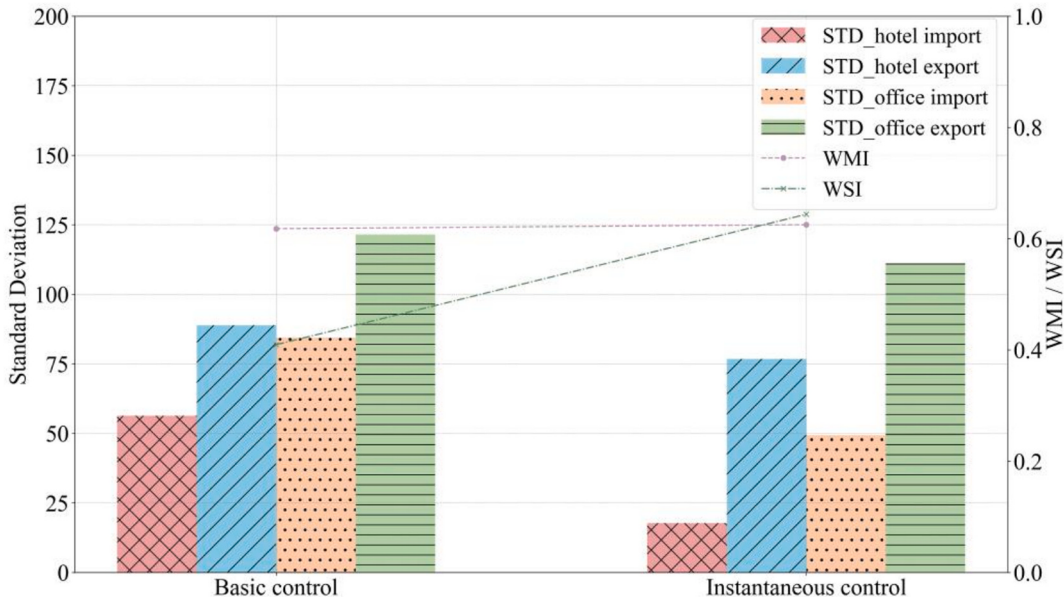


Fig. 12. System performance on grid stability and energy matching of representative case G8C38.

to the benchmarks than the initial inputs. The cross rate and mutate rate of the genetic algorithm model are set as 0.8 and 0.4, respectively.

The predictive control methodology is developed based on the representative case mentioned in [Section 5.1](#). The system performance comparison of grid stability between basic control, instantaneous control, and predictive control can be seen in [Fig. 13](#). It is noticed that the developed genetic predictive control can provide further improvement for all four dimensions of grid stability, a further 7.2 % enhancement on grid stability than the instantaneous control is achieved by the genetic predictive control, enhancing the WSI from 0.643 to 0.689 on the representative case under the practical demand dataset.

According to the development process of genetic predictive control

as presented in this subsection, integrating genetic algorithms in the instantaneous control to form the predictive control method for grid stability is proven to be effective, and it can provide a noticeable improvement on the WSI than instantaneous control in the simulated cases. The recommended cross rate and mutate rate are 0.8 and 0.4 for the genetic algorithm in the predictive control. The generation number is set as 6000 and it can be modified based on the computing resources and the expected improvement and time costs. Enlarging the generation number may bring better stability performance but there may be more computational challenges. The generation number could also be slightly reduced with some enhancement sacrifice when the computing resources are limited.

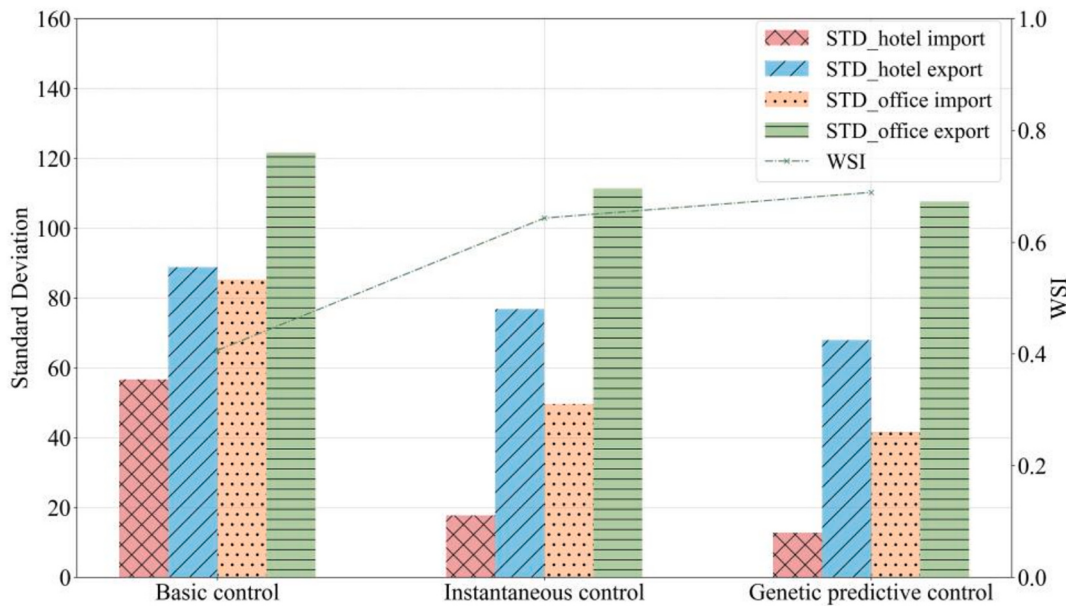


Fig. 13. Grid stability performance between different controls under practical dataset on the representative case G8C38.

5.3. Genetic predictive control for grid stability: The impact of ocean renewable energy systems

With the implementation of the genetic predictive control methodology developed in Section 5.2, cases in Group 27 with different renewable energy combinations, as mentioned in Table 3, are simulated under the practical building demand dataset. The impacts of different types of ocean renewable energy systems on the system performance under predictive control and enhancement compared with instantaneous control are investigated.

The system performance of twenty-five cases just with FPV and OWT in Group 27 is illustrated in Fig. 14. Compared with the performance in Fig. 7 under instantaneous control, the trends under predictive control are similar. Regarding the grid stability, 100 % penetration of solar energy still shows a 20.2 % higher WSI than 100 % wind energy (0.595 vs 0.495). The reasons may still be the dominant daytime demand of the system, and the extra fluctuation brought by excessive wind energy in the nighttime, similar to that under instantaneous control. Introducing an appropriate ratio of wind energy to the system results in a better stability performance. The case with OWT to FPV ratios of 25%:75% for the office and 50%:50% for the hotel shows the highest WSI of 0.678 among the twenty-five cases. A similar trend can also be noticed when analyzing the energy matching in Fig. 14 (b). The case fully relying on solar energy shows better energy-matching than the case with 100 % OWT, having a 20.2 % higher WMI (0.511 vs 0.425). Also, mixed systems with appropriate wind and solar energy that align with the characteristics of the demand can provide better matching performance than implementing one type of renewable energy individually. The case with the best stability performance also shows the highest WMI of 0.613, of which the OWT to FPV ratio for the office is 25%:75%, and that ratio for the hotel is 50%:50%. As for the economic performance, the trend is also clear and similar to that under instantaneous control. The OWT shows higher economic benefits than FPV on a 20-year scale. The case with 100 % penetration of the OWT shows 54.218 million HKD NPV_{rel} , 30.675 million higher than the case with 100 % FPV. Introducing FPV to a system with 100 % OWT will sacrifice the economic benefits gradually. As the genetic predictive control is developed based on the instantaneous control and its objective is to obtain better grid stability performance, the enhancement of the twenty-five cases under genetic predictive control on WSI compared with those with instantaneous control under the practical demand datasets are analyzed as shown in

Fig. 14 (d). Note that the cases with lower WSI under instantaneous control as shown in Fig. 7 (a) have better improvement under genetic predictive control. The largest enhancement (13.8 %) happens in the case with 100 % OWT. The average enhancement of these cases is 8.5 %, ranging from 6.5 % to 13.8 %.

When considering introducing Tidal energy, the eight cases with TSGs are analyzed in Fig. 15. As shown in the figure, the trends of the impact of TSGs on grid stability, energy matching, and economic performance under genetic predictive control are similar to those under instantaneous control. When considering TSG with OWT, an increase of TSG modules will first help improve the grid stability then decrease it. The case with two TSG modules has the highest WSI 0.528 among the four cases. The trend is also the same when considering TSG with FPV. As for the energy matching, a similar trend is noticed in Fig. 15 (b), which states that introducing tidal energy will also first improve the matching and then decline it under predictive control. Among the four cases just with TSG and OWT, the case with four TSG modules has the highest WMI 0.467. When considering cases just with TSG with FPV, the highest WMI of 0.574 also comes from the case with four TSG modules. As shown in Fig. 15 (c), TSG shows clearly poorer economic performance on a 20-year scale than both OWT and FPV. When considering TSG with OWT only, utilizing six modules of TSGs will sacrifice 32.797 million HKD NPV_{rel} compared with the case with 100 % OWT. When considering TSG with FPV, the trend is also the same, implementing six TSG modules sacrifices 18.034 million HKD NPV_{rel} than the case with 100 % FPV. As for the enhancement of grid stability compared with instantaneous control, it is noticed that the trend is similar to that among the cases just with OWT and FPV mentioned above, which is that the cases with poorer grid stability performance under instantaneous control have better improvement under genetic predictive control. As shown in Fig. 15 (d), when only considering TSG with OWT, the case with six modules of TSGs shows the highest enhancement of 15.3 %. The highest enhancement 10.8 % also comes from the case with six TSG modules while considering TSG with FPV. Among the 8 cases with implementation of TSG and supplemented by only OWT or only FPV, the average enhancement on grid stability than instantaneous control is 11.2 %, ranging from 7.8 % to 15.3 %.

The impacts of implementing different types of ocean renewable energy systems under genetic predictive control on the performance of the system in different aspects are analyzed in this subsection. Similar to outcomes from cases under instantaneous control, FPV systems show

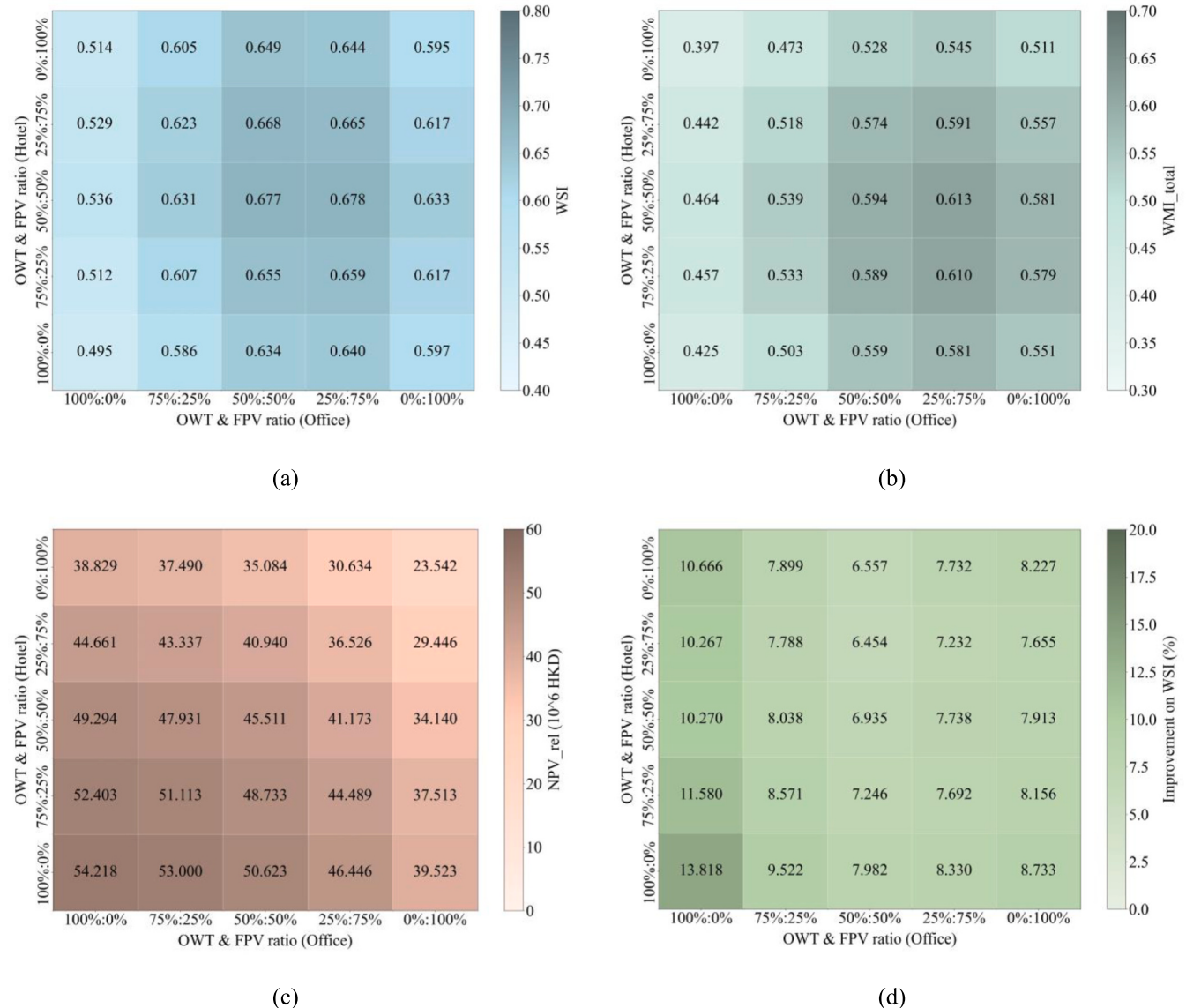


Fig. 14. System performance of cases in Group 27 with different proportions of OWT and FPV regarding (a) Grid-interaction stability, (b) Energy matching, (c) Relative net present value, and (d) Enhancement of stability than instantaneous control.

better technical performance than OWT systems when considering introducing only one type of renewable energy. Mixed systems still show significantly better technical performance. The suggestions for the design of coastal ZEBs under the predictive control derived from the results are generally similar to those under the instantaneous control. The penetration ratios from 50%:50% to 25%:75% for offshore wind and solar energy are still recommended for renewable energy systems design for coastal ZEBs depending on the demand characteristics. As for economic performance, OWT brings more benefits than FPV and both of them are better than TSG. When introducing TSG into the systems, around a 30% penetration level for the hotel is still recommended for relatively better technical performance and acceptable economic loss. Besides, for the systems with lower WSI under instantaneous control, implementing the predictive control can bring a relatively higher enhancement.

5.4. Predictive control for road impact and grid stability

After developing the genetic predictive control algorithm, the road impact of EVs commuting between two buildings is taken into account,

and a predictive control strategy for both road impact and grid stability is developed as described in Section 3.3.3. This strategy integrates predictive schedule selection and genetic control of EV charging and discharging power 24 h in advance. The PRI, NRI, and ORI introduced in Section 4 are used to assess the road impact.

The commute route between the hotel and office buildings is divided into five sections in this study, where each section has a 5 km distance. The historical road congestion factors of each section used in this study come from Google Maps and are categorized into levels 1, 2, 3, and 4, where 4 indicates extreme congestion, 3 indicates moderate congestion, 2 indicates moderate smoothness, and 1 indicates very smooth traffic. The time resolution of historical data is 0.25 h, the same as the simulation timestep. The corresponding drive time needed for each section under four levels of congestion conditions is five, six, ten, and fifteen minutes respectively, calculated based on Google Maps. In terms of practical road information datasets, the stochastic method similar to that for practical demand data is used based on the historical road congestion datasets. Deviation factors ranging from -1 to 1 following normal distribution are added to the historical road congestion factors of every timestep. The drive time needed for each section under practical

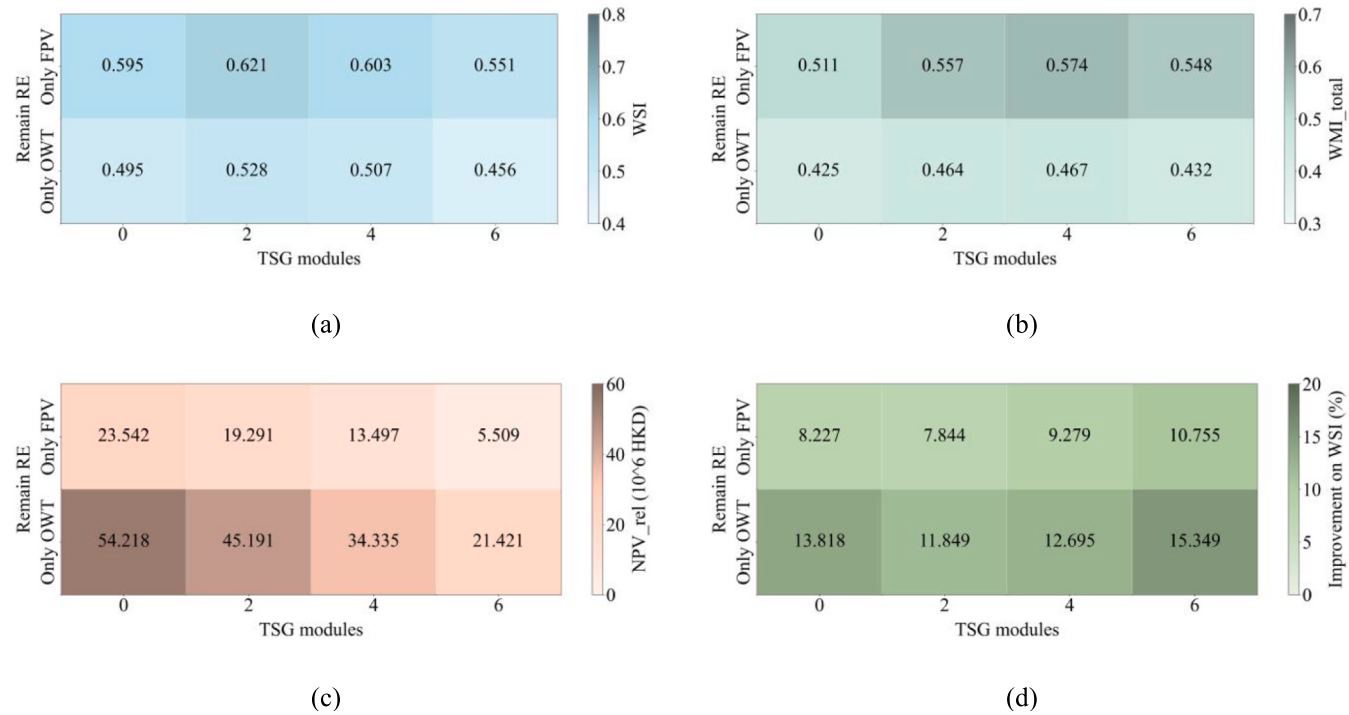


Fig. 15. System performance of cases in Group 27 with the implementation of TSG regarding (a) Grid-interaction stability, (b) Energy matching, (c) Relative net present value, and (d) Enhancement of stability than instantaneous control.

road congestion factors is calculated based on the drive time under historical factors using the linear interpolation method. To investigate the impact of stochastic levels on the road impact of the predictive control, five practical road congestion datasets with standard deviations of 0.1, 0.2, 0.3, 0.4, and 0.5 for normally distributed deviation factors are generated and investigated in this section. The control strategy utilizes averaged historical road information to make the decision, expecting to mitigate the variance of individual timestep between

historical and practical data. Hence, different historical road information averaging levels from 0.25 to 1.75 h are investigated in this section. The cases in this section share the same practical demand datasets as those in Sections 5.2 and 5.3. As for the renewable energy design, three combinations on the Pareto front shown in Fig. 9 are selected for this section, which are combinations 14, 29, and 38.

As shown in Fig. 16, the practical ORI under different historical data averaging levels and practical data stochastic levels and the

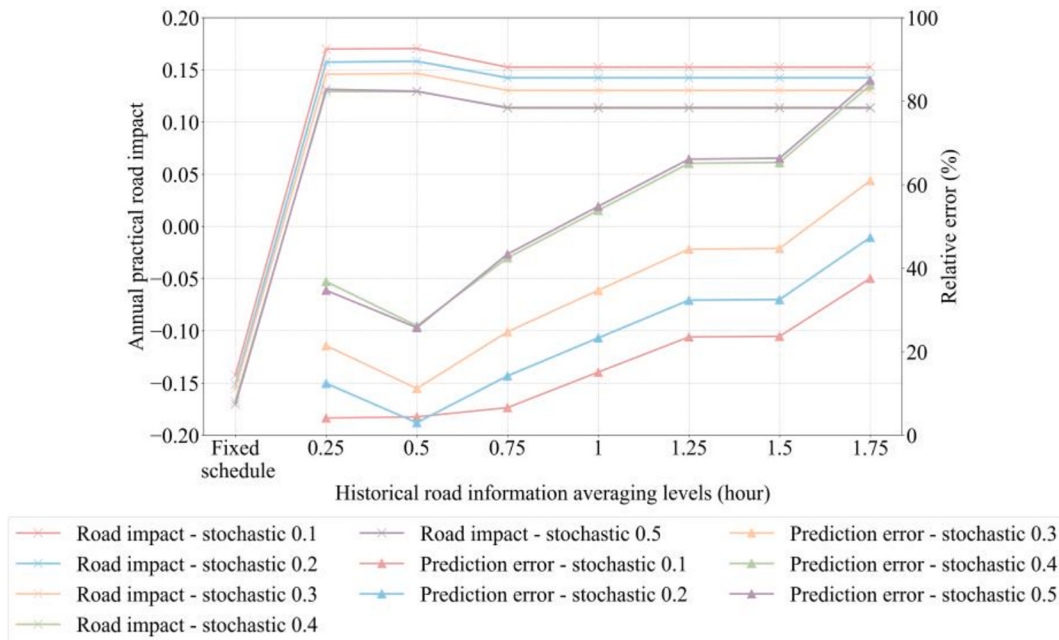


Fig. 16. Annual ORI and prediction errors of predictive control for road impact and grid stability under different historical averaging levels and practical stochastic levels.

corresponding relative prediction errors compared between predicted annual ORI and practical annual ORI are investigated. In terms of the prediction error, a noticeable improvement is shown when increasing the historical road data averaging levels from 0.25 to 0.5 h while the stochastic levels are larger than 0.1, and the reduction of relative error ranges from 8.9 % to 10.6 %. The reason may be that when there is a relatively larger difference between practical and historical road information, using averaged historical data of an appropriate level to predict the practical condition can mitigate the variance between practical and historical information, resulting in better accuracy than just using instantaneous historical information. Under the stochastic level 0.1, the prediction relative error slightly increases from 4.1 % to 4.4 %, due to that the difference between practical and historical road congestion conditions is small and just using the instantaneous historical information to predict can have the best accuracy, and using averaged historical data will introduce more variance into the prediction. Under all stochastic levels, further increasing the averaging level to larger than 0.5 h, the prediction accuracy will all be poorer, meaning that regardless of what stochastic levels, using averaged historical road information of levels larger than 0.5 h will all introduce extra error rather than mitigating the variance between historical and practical information. Under the averaging level of 0.5 h, the relative errors under different practical datasets range from 3.0 % to 26.2 %, with an average of 14.1 %, which is the lowest average prediction error among all historical data averaging levels. As for the practical ORI under predictive control, significant improvements compared with the fixed EV schedules of other controls are noticed under all practical datasets. Under the fixed EV schedule, the average annual ORI under five practical road datasets is -0.16, meaning that on the annual scale, the commuting and energy-sharing behavior of EVs heaves the road congestion condition. After the implementation of predictive control considering road impact, the average annual practical ORIs of five practical datasets were improved to a range between 0.13 and 0.15 under different historical data averaging levels, meaning that

the predictive control improves the impact of EVs on the road from heaving the congestion to enhancing the road utilization on an annual scale. Under the historical data averaging level of 0.5 h which shows a better prediction accuracy, the annual practical ORI ranges from 0.13 to 0.17 under different stochastic levels, with an average ORI of 0.15.

To investigate the impact on grid stability of considering road impact, the grid stability comparisons shown in Fig. 17 are based on the cases with combinations 14, 29, and 38 under instantaneous control and genetic predictive control with a fixed schedule, and genetic predictive control with predictive schedule, which are control 1, control 2, and control 3, respectively. Regarding the part of road impact control, the practical road information dataset with the stochastic level of 0.1 and historical data averaging level of 0.5 h are selected as representative stochastic level and historical data averaging level for the cases shown in Fig. 17. As shown in Fig. 17, the trend of grid stability is similar under three combinations. Implementing genetic predictive control can bring significant improvement to grid interaction stability. Under the two kinds of predictive controls, whether using a predictive schedule taking road impact into account will not bring a noticeable influence on the grid interaction stability, while the WSI remains almost the same. Under combination 14, the WSI is improved from 0.629 to 0.678 by 7.8 % when introducing genetic predictive control and remains at 0.678 after taking road impact into account. The WSI of combination 29 under the three kinds of controls are 0.624, 0.674, and 0.675, and that of combination 38 is 0.643, 0.690, and 0.690. This indicates that integrating road impact control into genetic predictive control can still benefit grid stability while improving road impact significantly.

This subsection presented the analyses for the predictive control integrated with grid stability and road impact control. The road impact control relies on the predictive schedule selection method based on averaged historical road information. Performance on prediction accuracy of different historical data averaging levels under various stochastic practical datasets is analyzed, and the recommended historical road

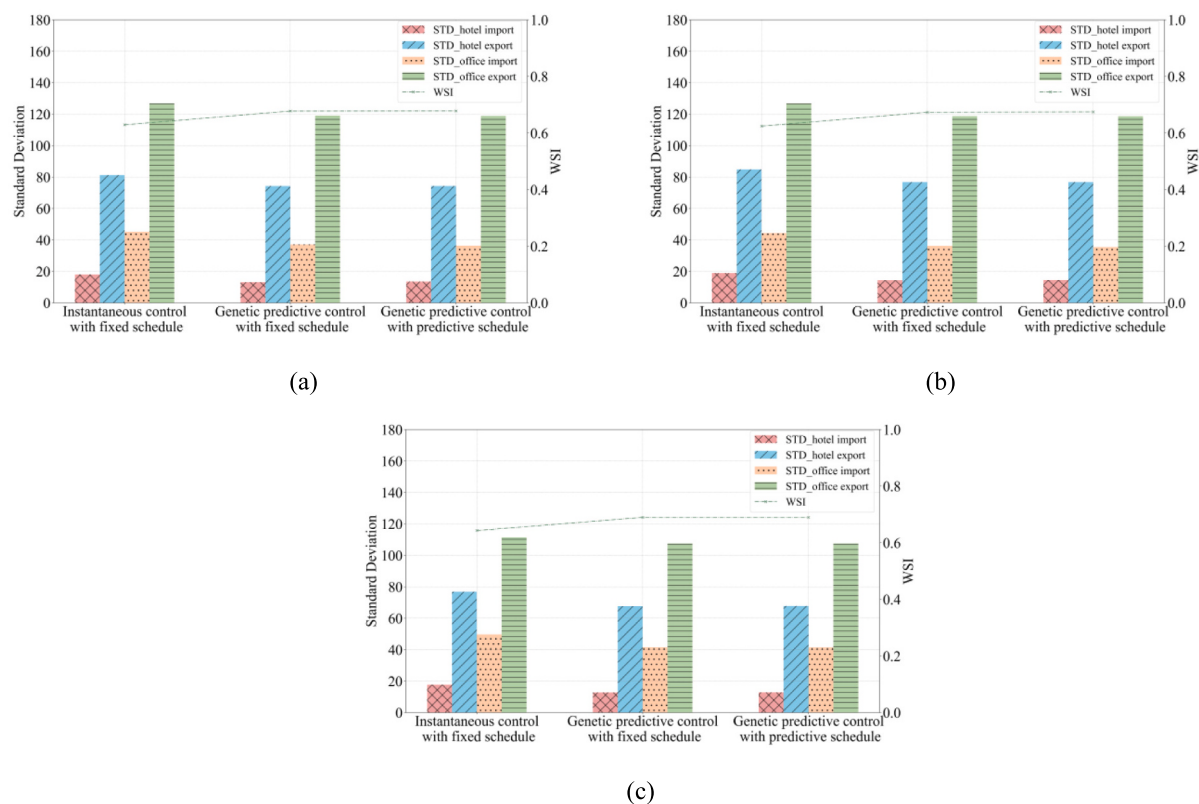


Fig. 17. Grid stability performance under three controls with three representative combinations including (a) Combination 14, (b) Combination 29, and (c) Combination 38.

information averaging level is 0.5 h derived from this study. By implementing the predictive control considering road impact, the annual overall road impact of ZEVs in the zero-energy system can be improved from heavying the congestion to enhancing the utilization of road resources. Moreover, integrating road impact control into the genetic predictive control still can help the system enhance the grid stability performance by a similar level.

5.5. Implementation strategies

After comprehensively analyzing the performance of the hybrid zero-energy system under different renewable energy design options and various control strategies. Several suggestions about the implementation strategies for similar coastal zero-energy systems are provided in this subsection in terms of the design and control aspects. Regardless of the control approach, solely implementing FPV systems performs better in technical aspects than solely introducing offshore wind energy while OWT has a better economic performance on a 20-year scale. Other than implementing one type of renewable energy only, mixed usage of offshore wind and solar energy in a ratio of 50 %:50 % to 25 %:75 % shows a significantly better technical performance in both instantaneous control and predictive control. When considering tidal stream energy, compared to wind and solar energy, TSG shows a poorer economic performance. However, introducing TSG to cover around 30 % of the demand for buildings similar to hotels with noticeable nighttime demand can help the system enhance the technical performance significantly under instantaneous and predictive controls while the economic sacrifice is at an acceptable level. Considering the grid stability performance, the implementation of genetic predictive control can bring a further enhancement to the system than the instantaneous control, and the enhancement is more obvious for the systems with lower stability performance originally. In the genetic predictive control strategy, the generation number can be modified depending on the computing resources, expected enhancement level, and tolerable time consumption level. For the systems located in congested cities, introducing the road impact control part into the predictive control can significantly improve the annual road impact of ZEVs in the systems from heaving the congestion to enhancing the usage of road resources, while the enhancement of grid stability is not sacrificed. In the road impact predictive control, the averaging level of historical road information is recommended to be set as 0.5 h with the best prediction accuracy performance based on this study.

6. Discussion of the broader implications, limitations, and future directions

In order to investigate the applicability of the findings presented in Section 5 and the sensitivity of the system performance on different variables, more scenarios are implemented on the representative case from Section 5, regarding deviations of energy generation, building demand, and economic parameters, and the results and discussion are presented in Section 6.1. Moreover, to study the applicability of the developed control approach for grid stability for ZEBs out of coastal areas, a change of scenario from coastal area to inland area is also simulated and analyzed in Section 6.1. Following that, Section 6.2 discussed the possibility of expanding the system scale and the corresponding potential computational challenges and time costs of the control approaches. Besides, some limitations of this study and future research directions are discussed in Section 6.3.

6.1. Applicability of the methods and findings

To examine the applicability of the representative renewable energy combination under different scenarios. Sensitivity analysis for the representative case G8C38 from Section 5.1 on different parameters is conducted and presented in this part. First, the deviations of wind and

solar energy generations are considered and their impact on the techno-economic performance of the representative case is investigated. As shown in Fig. 18, the impact of individual deviation of solar or wind energy from -10 % to 10 % with a 2 % step on the system's techno-economic performance is analyzed. In terms of the grid stability performance, a decrease in renewable energy generation in the presented range can generally enhance the stability control, due to that less renewable energy will introduce fewer fluctuations for the system and then improve the stability performance. Comparing wind to solar energy, the change of wind energy has a higher impact on the system interaction stability due to wind energy may bring more fluctuations into the system. From the deviation from -10 % to +10 %, solar energy causes a reduction of WSI by 1.8 % from 0.649 to 0.637, while the reduction from wind energy is 3.2 % from 0.654 to 0.633. As for the energy-matching performance, different from WSI performance, an increase of solar energy in the deviation range can slightly improve the matching performance due to that the major demand of the system occurs in the daytime, aligning with the solar energy characteristic. Slightly increasing solar energy can cover more daytime demand for the system to enhance the matching performance. From the deviation from -10 % to +10 %, solar energy can enhance the WMI by 1.0 % from 0.622 to 0.628. Conversely, because of the feature of wind energy, an increase in it will bring extra energy at nighttime without enough demand and bring more exported energy for the system to decline the energy-matching performance. The deviation from -10 % to +10 % of wind energy brings a decrease in WMI by 0.8 % from 0.628 to 0.623. When considering the economic benefits, because of the FiT subsidy, the decrease in renewable energy directly sacrifices the NPV_{rel} . Comparing solar to wind energy, decreases in solar energy will also decrease the energy-matching as mentioned before to sacrifice the saved imported energy cost. Hence, economic benefits show more sensitivity to deviations of solar energy than wind. From +10 % to -10 %, the decrease in solar energy brings a reduction of 9.206 million HKD on NPV_{rel} and the reduction from the decrease in wind energy is 7.739 million HKD. Besides the individual deviation of one type of generation, the impact of simultaneous deviations for solar and wind energy from -10 % to +10 % with a step of 5 % on the system's techno-economic performance is also investigated as illustrated in Fig. 19. As shown in Fig. 19 (a), the impact on stability performance shows the same trend as Fig. 18, and wind energy shows a more significant negative effect on WSI than solar energy. The case under higher wind with lower solar energy scenario with +10 % wind energy deviation and -10 % solar energy deviation presents a 1.5 % lower WSI than the scenario of lowest wind and highest solar energy (0.638 vs 0.648). The trend for energy-matching in Fig. 19 (b) is also similar to that in Fig. 18. A slight increase in solar energy will benefit the matching performance and that in wind will decline it. The case under the +10 % solar and -10 % wind energy scenario shows the highest WMI of 0.631 among the twenty-five cases, 1.9 % higher than the case with -10 % solar and +10 % wind energy. Similarly, economic benefits show higher sensitivity to deviations of solar energy, the case with the highest solar and lowest wind energy shows a 0.598 million HKD higher NPV_{rel} than the case under the converse scenario.

Second, the impact of deviations in building demand on the system's techno-economic performance is also studied in this subsection. As shown in Fig. 20, decreases in building demand first improve the stability performance, and then the WSI keeps at a stage. Similar to the impact of generation, slightly decreasing the building demand will reduce the fluctuations in excessive and shortage power of the system to a certain value. Further decrease in the demand may increase the fluctuations gradually to the extreme condition that with pure generation fluctuations. From +15 % to -12 %, the deviation of building demand brings a 15.5 % enhancement on WSI. In terms of energy-matching, decreases in building demand will result in more excessive renewable energy that needs to be exported, and result in a lower WMI. The case with +15 % demand shows a 6.8 % higher WMI than -15 % demand. Regarding the economic benefits, as the indicator is the relative net

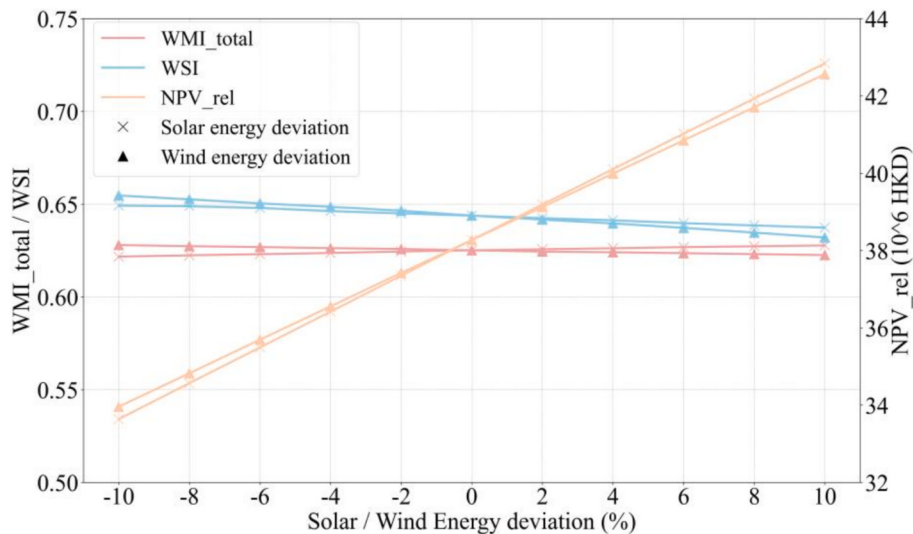


Fig. 18. Sensitivity analysis for individual solar or wind energy deviation.

present value, with increasing the building demand from -15% to $+15\%$, the improved energy matching performance means the higher saved imported energy cost and helps increase the NPV_{rel} by 20.3 %.

Third, this subsection also presents the impact of changes in economic parameters on the economic benefits. The impacts of changes in the interest rate and the electric tariff are illustrated in Fig. 21 (a), as shown in the diagram, increasing the interest rate significantly declines the NPV_{rel} . Under the extreme scenario with a 10 % interest rate, the system presents a negative NPV_{rel} of -2.312 million HKD. As the indicator is the relative net present value, increasing the electric tariff will significantly enhance the saved imported energy value and help increase the NPV_{rel} . From -30% to 30% , the increase in the electric tariff helps enhance the NPV_{rel} by 70 %. Fig. 18(b) demonstrates the impact of changing investment costs for key renewable energy systems on the economic benefits. As shown in the diagram, based on the representative case, the deviation in FPV investment cost shows the highest impact on economic benefits, followed by OWT. The impact of TSG investment cost is minimum due to TSG only supports the hotel and has a lower penetration level to the system than FPV and OWT. From -20% to 20% , the increase in FPV investment cost brings a 31.0 % reduction on NPV_{rel} , while those from OWT and TSG investment cost increases are 18.7 % and 16.0 % respectively.

Besides, in order to examine the applicability of the developed instantaneous and genetic predictive control approaches for grid stability for ZEBs out of coastal areas. The study changes the scenario of the representative case from coastal areas to inland areas. Instead of Floating PV systems, BIPV for the two buildings is implemented in the inland scenario, and PV panels are supposed to be installed at 60 % area of the rooftop and all four facades except the window areas. The offshore wind turbine system is supposed to be changed to inland wind turbines, with the ground roughness changing from 0.06 of open water to 0.10 of short grasses. TSG modules are removed in the inland scenario. Other parameters and weather files remain the same as the original representative case. After changing the scenario, basic control, instantaneous control, and genetic predictive control for grid stability are implemented in the inland cases to investigate the applicability of the developed approaches. The results of the inland cases on grid stability performance are presented in Fig. 22. As shown in the diagram, the stability performance of both the import and export sides of both hotel and office buildings is improved with instantaneous control and further enhanced after implementing genetic predictive control. The WSI of the inland system increases by 45.5 % with the instantaneous control. A further enhancement of 9.8 % on WSI than instantaneous control can be

achieved by genetic predictive control, even higher than the enhancement achieved under coastal area (7.2 %) mentioned in Section 5.2. The results indicate that the control approaches for stabilizing the grid interaction are applicable to ZEBs in inland areas. Regarding the road impact control part, as the change of scenario from coastal to inland area will not influence the behaviors of EVs much, the road impact control is considered to be applicable to inland ZEBs and the performance can refer to Section 5.4.

6.2. Scalability of the proposed methods

This study proposes instantaneous and predictive control approaches using TRNSYS combined with Python for a hybrid zero-energy system consisting of two ZEBs and 20 zero-emission vehicles. The scalability of the developed control methods to a larger zero-energy system is considered and investigated in this section. The possibility of implementing the developed approaches to larger-scale systems and the corresponding potential computational challenges and time costs are discussed.

In terms of the feasibility of the control approach for larger scale systems, it is generally feasible when the system has energy imbalance and instability problems and has battery resources including ZEVs or building batteries. On the one hand, if the larger zero-energy system consists of various types of buildings with different demand characteristics, the larger scale can help the whole system be more stable than individual buildings due to the different periods of peak and valley demand. Then scaling up the system can facilitate both the instantaneous and predictive control methods for grid interaction stability. On the other hand, when the larger zero-energy systems consist of buildings with similar demand characteristics, the stability of the whole system may decline compared to small-scale systems due to the synchronized peak and valley demand periods. Then the efficiency of the control approaches for grid stability may be reduced if there are no extra battery resources compared to small-scale systems.

As for the potential computational challenges of the developed control approaches using dynamic simulations in larger scale systems, compared to predictive control, the instantaneous control method may not have concerning problems as it makes decisions based on instantaneous signals and just scaling up the system will not increase the computation complexity much. Regarding the genetic predictive control method, as the decision from it is provided based on the dynamic simulation results with the genetic algorithm for the several groups of batteries of the prediction window, the key factor affecting the

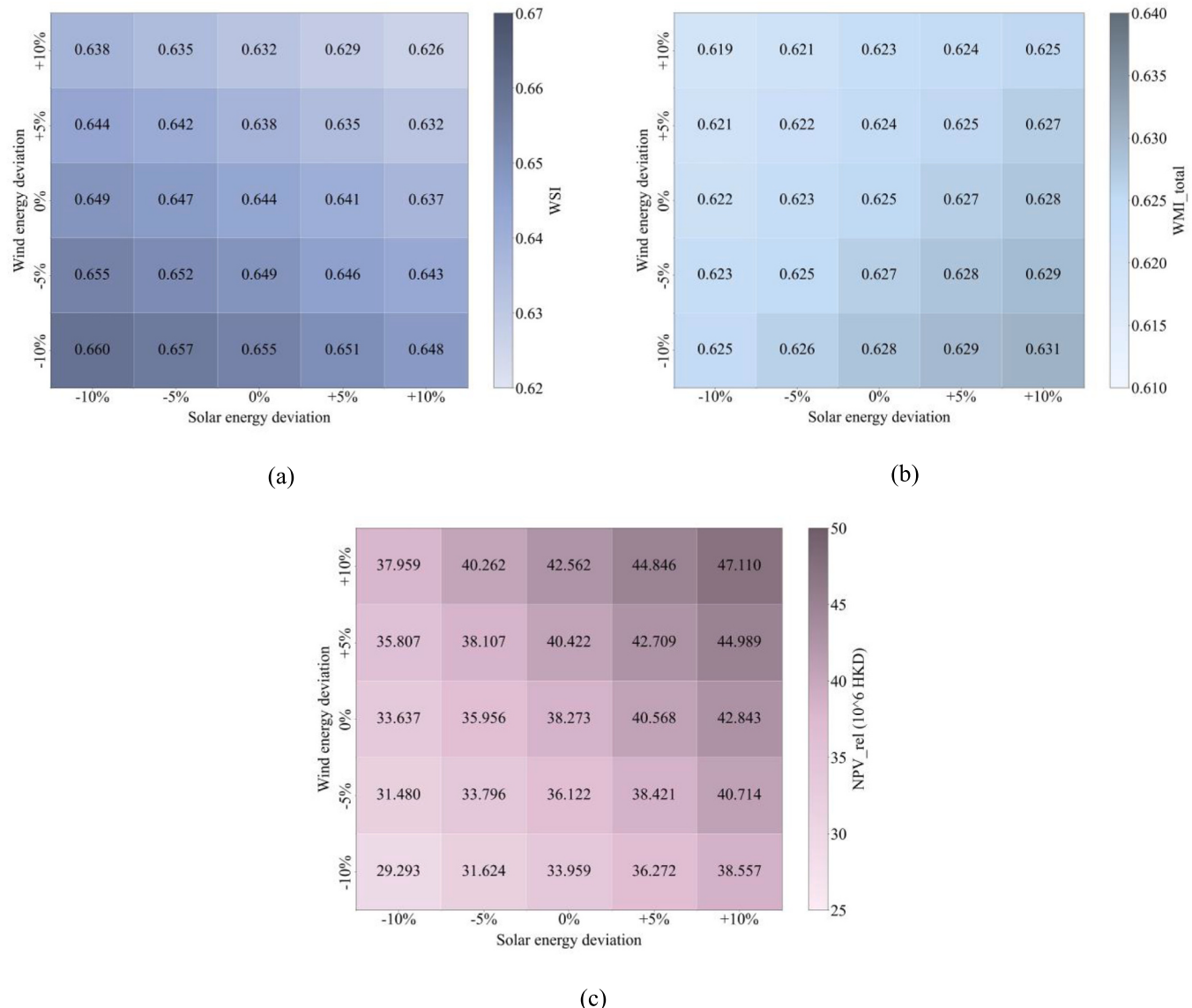


Fig. 19. Sensitivity analysis for simultaneous solar and wind energy deviation regarding (a) Grid-interaction stability, (b) Energy matching, and (c) Relative net present value.

simulation computational time is the number of groups of batteries rather than the scale of the system. In other words, a large-scale system with large amounts of buildings and ZEVs but the battery resources are divided into several control groups may not meet serious computational challenges. However, if the battery resources of the system are divided into more groups that need various control signals, the genetic algorithm may need more generations and take more time to get an equivalent relative better performance as presented in this study. Besides, large-scale systems may introduce multiple stakeholders instead of one stakeholder. Then the genetic predictive control may need more computational resources and time to calculate and balance the benefits for different stakeholders.

6.3. Limitations of the study and future directions

While this study conducts techno-economic analyses for different renewable energy resources supporting coastal ZEBs and proposes feasible control approaches to stabilizing grid interaction and alleviating negative road impact, several limitations need to be acknowledged for comprehensively understanding the research outcomes and proposing

future research directions. Limitations regarding types of buildings and vehicles, the scale of the system, and the climate condition and corresponding potential future directions are discussed in this subsection.

First, the analyses of this study are based on a hybrid zero-energy system consisting of hotel and office buildings, and twenty ZEVs with 85 kWh battery capacity each. Although two kinds of buildings with different demand characteristics are considered, various building types with other demand characteristics are not covered in the study, such as public buildings, industrial buildings, etc. This may limit the applicability of the research findings on the systems with other building types having demand characteristics different from hotels and buildings. Moreover, only one type of ZEV is studied in the research, the performance of the developed control approaches on systems with other types of ZEVs such as electric buses or electric trucks with larger battery capacity and different schedules, can not be accessed from this study. Hence, introducing more types of buildings with various demand characteristics and more types of ZEVs into the studies on zero-energy systems is valuable for future research.

Second, this study focuses on the performance of a system with two buildings and twenty ZEVs, although sensitivity analyses for small-scale

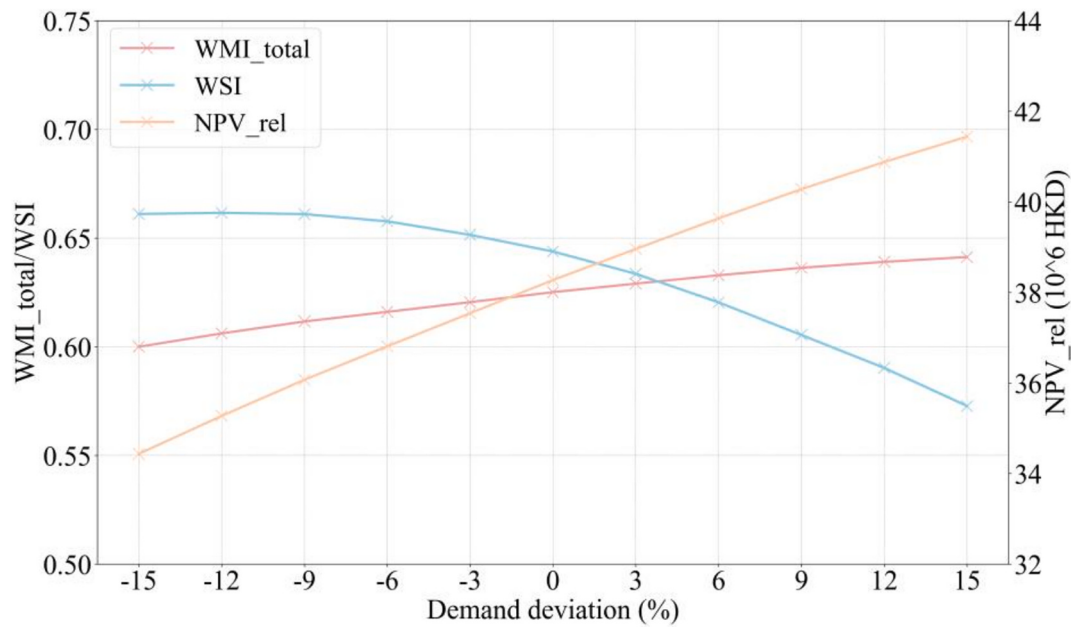


Fig. 20. Sensitivity analysis for building demand.

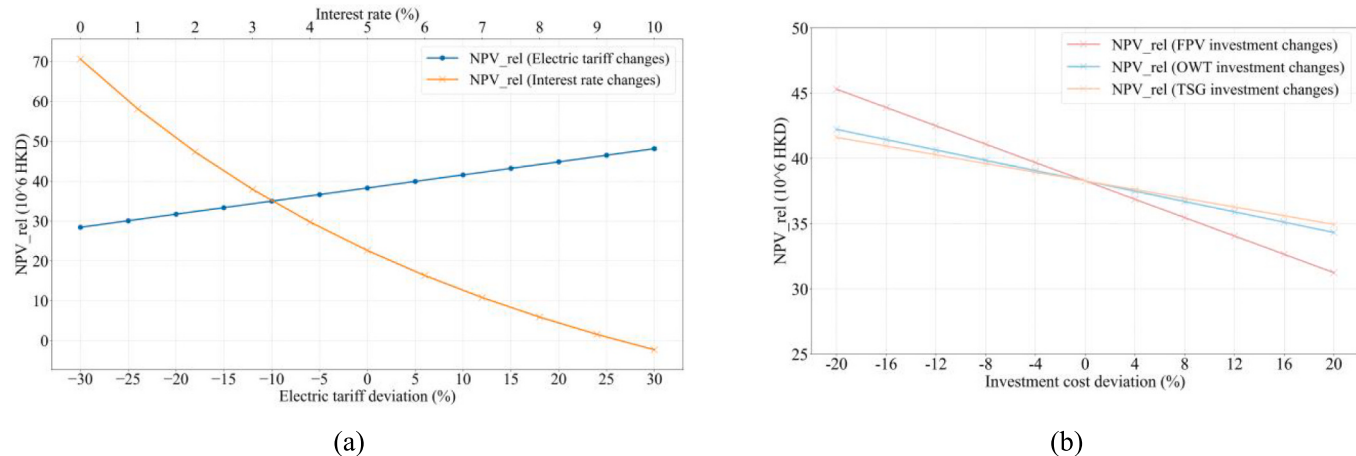


Fig. 21. Sensitivity analysis for economic parameters including (a) Interest rate and electric tariff, and (b) Investment cost.

energy generation and building demand deviations are conducted in Section 6.1, and the scalability of the proposed methods is discussed in Section 6.2, the specific performance and analyses of much larger systems are not provided in this research. This limits the comprehensive understanding of the detailed performance of large-scale zero-energy systems. More studies relating to introducing large-scale changes to the system with ZEBs and ZEVs can be done in the future to facilitate the understanding of the specific impact of scaling up the system and the potential corresponding design and control solutions.

Third, the analyses in this study are based on the climate condition of Hong Kong SAR, which is a city with a cooling-dominated climate and the imbalance between weather of different seasons is moderate. The performance of the proposed system under other types of climate conditions is short of understanding and still needs to be investigated. This may limit the understanding of specific design suggestions and control solutions for ZEBs in different climate conditions. In the future, studies can extend to other types of climate conditions including heating-dominated climates and climates with much more seasonal imbalance to facilitate the understanding of the design and control for zero-energy systems in various regions of the world.

7. Conclusions

With the increasing penetration of zero-emission vehicles, renewable energy systems, and ZEBs, using EV-based energy-sharing methods to form a carbon-neutral system with ZEBs and to enhance on-site renewable energy usage attracts increasing attention in academia and industry. However, the grid-interaction fluctuation issue introduced by renewable energy in such systems has not been comprehensively investigated. Meanwhile, predictive control methods considering grid-interaction performance were less utilized in previous control strategies developed. Also, the negative road congestion impact brought by the zero-emission vehicles (ZEVs) used for commuting and sharing energy was rarely covered in past studies. Based on these scientific gaps, the study investigates instantaneous and predictive control strategies for the ZEV-based energy-sharing method, considering both grid-interaction stability and reducing negative road impact in a carbon-neutral hybrid system with ZEBs. In the simulation-based study, various groups of cases with different renewable energy system combinations and control strategies are analyzed. Based on the analysis, several conclusions are drawn.

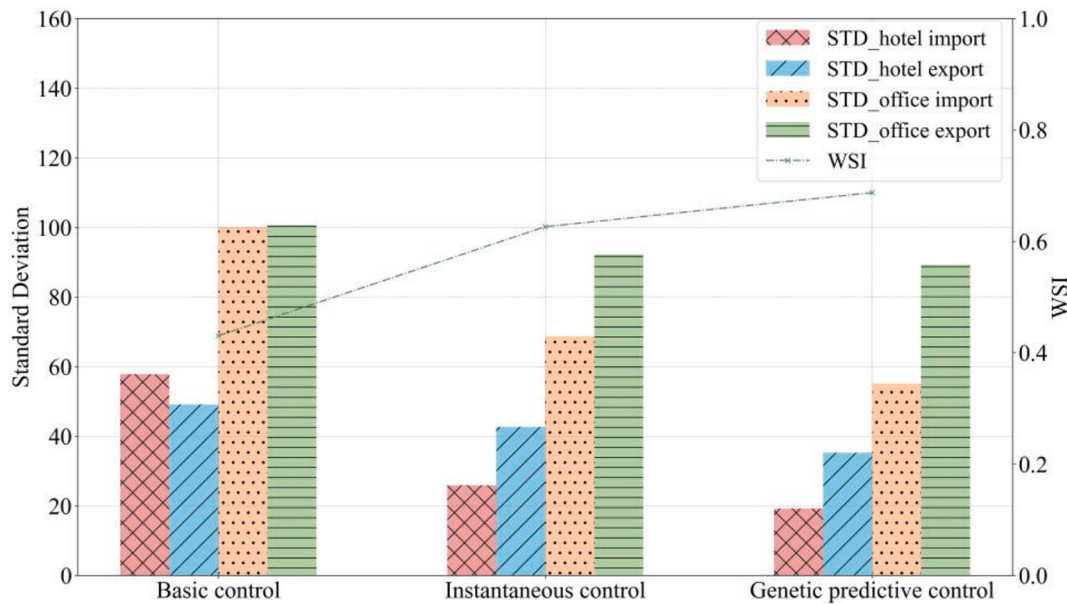


Fig. 22. Grid stability performance between different controls under the inland scenario.

First, under the weather conditions of Hong Kong, solely implementing Floating PV systems in common ZEBs like hotels and offices shows better technical performance on grid-interaction stability and energy matching than solely implementing OWT. Using WSI and WMI as indicators, it has 26.4 % better grid-interaction stability and 17.4 % better energy-matching performance. However, FPV shows poorer economic performance than OWT on a 20-year scale, considering the installation and maintenance costs. The system fully relying on FPV has a 31.639 million HKD lower NPV_{rel} than that with only OWT. For a system with 100 % FPV, introducing an OWT system to cover 25 % to 50 % of the total demand can significantly improve technical and economic performance simultaneously. At the base of the system with FPV or OWT, introducing TSGs into the system to cover 30 % of the demand of the located building can bring better technical performance with an acceptable economic sacrifice. A mixed renewable energy system with equally distributed solar, wind, and tidal energy is recommended for the ZEB system in the study as it is on the Pareto front considering both technical and economic performance among different renewable energy combinations.

Second, an innovative parameter benchmark for building import or export power is proposed. With the adjustment of import and export benchmarks for the building-grid interaction power, the system's instantaneous control can be considered as matching-inclined control or stability-inclined control. The fully matching-inclined control with setting the import and export benchmarks as zero shows a 21.5 % improvement in energy matching but shows 9.3 % poorer performance on grid stability than traditional basic control. Meanwhile, the stability-inclined control can show up to 71.0 % enhancement in grid stability, but the case with the best stability performance shows 23.8 % poorer energy-matching performance than traditional basic control. A benchmark group with original import benchmarks and 50 % of original export benchmarks is on the Pareto front among twenty-five benchmark groups and is selected as the representative benchmark group, and the case with it has a 57.1 % enhancement on grid-interaction stability and a 1.1 % improvement on energy matching than basic control, together with a 38.273 million HKD of 20-year relative net present value.

Third, for the representative case, a genetic predictive control algorithm is developed for better grid-interaction stability performance. Using historical energy data as input to the genetic algorithm model, the system can get the recommended charging and discharging power for batteries for the next twenty-four hours at the beginning of every day.

After implementing the genetic predictive control, a 7.2 % further enhancement can be achieved on the grid stability. The impact of changing ocean renewable energy types on the system performance under genetic predictive control is also investigated and the trend is similar to that under instantaneous control. As for the enhancement of grid stability, the system with a lower initial WSI shows higher relative enhancement. The enhancement presented in Section 5.3 between genetic predictive and instantaneous control averages 9.2 %, ranging from 6.5 % to 15.3 %.

Fourth, road impact is further considered in predictive control. Based on the developed genetic predictive control for grid stability, at the beginning of each prediction window, averaged historical road congestion data is utilized for the ZEV schedule decision for the next twenty-four hours. After integrating road impact control into genetic predictive control, the averaged annual ORI under practical road information datasets with different stochastic levels can be improved from -0.16 to a range from 0.13 to 0.15 using different historical road data averaging levels, which means the annual road impact of ZEVs for energy sharing and commuting is from heavying the road congestion to enhancing the road utilization during off-peak hours. The averaging level of 0.5 h shows the highest prediction accuracy in this study, the relative errors under different practical datasets are averaged at 14.1 %. After simulating three cases with various renewable energy combinations. The results indicate that integrating road impact into the genetic predictive control will not sacrifice the enhancement of grid-interaction stability.

This study proposes instantaneous and predictive strategies containing the EV-based energy-sharing method for system control of ZEBs, both considering grid-interaction stability and reducing negative road impact. Based on this preliminary study, some directions are interesting to be further investigated in the future, such as introducing more types of buildings with different demand characteristics and more types of ZEVs into the hybrid zero-energy system, studying the performance of proposed research findings to a system with much larger scale, conducting studies for the zero-energy systems in various areas with different climate conditions, etc. Besides, changing the prediction window of the predictive control, multi-objectives optimization control taking road impact and grid-interaction stability into account, and integrating machine-learning-based short-term prediction methods for road and energy information into the genetic predictive control may also be worth studying.

CRediT authorship contribution statement

Zhenyu Dou: Writing – review & editing, Writing – original draft, Methodology, Investigation. **Kai Pan:** Writing – review & editing, Writing – original draft, Methodology, Investigation. **Yang Xu:** Writing – review & editing, Writing – original draft, Methodology, Investigation. **Sunliang Cao:** Writing – review & editing, Writing – original draft, Supervision, Project administration, Methodology, Investigation, Funding acquisition, Conceptualization.

Declaration of competing interest

The authors declare that they have no known competing financial interests or personal relationships that could have appeared to influence the work reported in this paper.

Acknowledgment

This research is partially supported by the HK RGC (Hong Kong Research Grants Council) Research Project 15211822. This research is also partially supported by the Projects “P0044567” and “P0050992” from the Research Institute for Smart Energy (RISE), The Hong Kong Polytechnic University.

Data availability

Data will be made available on request.

References

- [1] The Long-Term Strategy of the United States: Pathways to Net-Zero Greenhouse Gas Emissions by 2050. <https://www.whitehouse.gov/wp-content/uploads/2021/10/us-long-term-strategy.pdf>; 2021.
- [2] China's Policies and Actions for Addressing Climate Change (2022). <https://english.mee.gov.cn/Resources/Reports/reports/202211/P020221110605466439270.pdf>; 2022.
- [3] Haider M, Davis M, Kumar A. Development of a framework to assess the greenhouse gas mitigation potential from the adoption of low-carbon road vehicles in a hydrocarbon-rich region. *Appl Energy* 2024;358:12235.
- [4] Ritchie H, Roser M. Cars, planes, trains: Where do CO₂ emissions from transport come from? Our world in data. 2024.
- [5] WorldGBC advancing net zero status report 2023. World Green Building Council; 2023.
- [6] Skaar C, Labonne N, Gradeci K. From zero emission buildings (ZEB) to zero emission Neighbourhoods (ZEN): A mapping review of algorithm-based LCA. *Sustainability* 2018;10:2405.
- [7] Salom J, Widén J, Candanedo J, Sartori I, Voss K, Marszal A. Understanding net zero energy buildings: evaluation of load matching and grid interaction indicators. *Proceed Build Simulation* 2011;2514–21.
- [8] Doroudchi E, Alanne K, Okur Ö, Kyrrä J, Lehtonen M. Approaching net zero energy housing through integrated EV. *Sustain Cities Soc* 2018;38:534–42.
- [9] Cao S, Hasan A, Sirén K. On-site energy matching indices for buildings with energy conversion, storage and hybrid grid connections. *Energ Buildings* 2013;64:423–38.
- [10] Barone G, Buonomano A, Calise F, Forzano C, Palombo A. Building to vehicle to building concept toward a novel zero energy paradigm: modelling and case studies. *Renew Sust Energ Rev* 2019;101:625–48.
- [11] Huang P, Lovati M, Zhang X, Bales C. A coordinated control to improve performance for a building cluster with energy storage, electric vehicles, and energy sharing considered. *Appl Energy* 2020;268:114983.
- [12] Barone G, Buonomano A, Forzano C, Giuzio GF, Palombo A, Russo G. Energy virtual networks based on electric vehicles for sustainable buildings: system modelling for comparative energy and economic analyses. *Energy* 2022;242:122931.
- [13] Cao S. Comparison of the energy and environmental impact by integrating a H 2 vehicle and an electric vehicle into a zero-energy building. *Energy Convers Manag* 2016;123:153–73.
- [14] Cao S. The impact of electric vehicles and mobile boundary expansions on the realization of zero-emission office buildings. *Appl Energy* 2019;251.
- [15] Zhou Y, Cao S. Investigation of the flexibility of a residential net-zero energy building (NZEB) integrated with an electric vehicle in Hong Kong. *Energy Procedia* 2019;158:2567–79.
- [16] Liu S, Cao S. Development of integrated energy sharing systems between neighboring zero-energy buildings via micro-grid and local electric vehicles with energy trading business models. *Appl Energy* 2025;380:124952.
- [17] Fachrizal R, Qian K, Lindberg O, Shepero M, Adam R, Widén J, et al. Urban-scale energy matching optimization with smart EV charging and V2G in a net-zero energy city powered by wind and solar energy. *eTransportation* 2024;20.
- [18] Shafiuallah M, Ahmed SD, Al-Sulaiman FA. Grid integration challenges and solution strategies for solar PV systems: A review. *IEEE Access* 2022;10:52233–57.
- [19] Eftekharnejad S, Vittal V, Heydt Keel B, Loehr J. Impact of increased penetration of photovoltaic generation on power systems. *IEEE Trans Power Syst* 2013;28:893–901.
- [20] Alquthami T, Ravindra H, Faruque MO, Steurer M, Baldwin T. Study of photovoltaic integration impact on system stability using custom model of PV arrays integrated with PSS/E. *North Am Power Symposium* 2010:1–8.
- [21] He P, Wen F, Ledwich G, Xue Y, Huang J. Investigation of the effects of various types of wind turbine generators on power-system stability. *J Energy Eng* 2015;141.
- [22] Adetokun BB, Muriithi CM, Ojo JO. Voltage stability assessment and enhancement of power grid with increasing wind energy penetration. *Int J Electr Power Energy Syst* 2020;120.
- [23] Schmiendorf K, Peinke J, Kamps O. The impact of turbulent renewable energy production on power grid stability and quality. *The Eur Phys J B* 2017:90.
- [24] Onar OC, Khaligh A. Grid interactions and stability analysis of distribution power network with high penetration of plug-in hybrid electric vehicles. In: 2010 Twenty-Fifth Annual IEEE Applied Power Electronics Conference and Exposition (APEC); IEEE; 2010.
- [25] Sayed MA, Ghafouri M, Atallah R, Debbabi M, Assi C. Grid Chaos: An uncertainty-conscious robust dynamic EV load-altering attack strategy on power grid stability. *Appl Energy* 2024;363:122972.
- [26] Wu D, Chau KT, Liu C, Gao S, Li F. Transient stability analysis of SMES for smart grid with vehicle-to-grid operation. *IEEE Trans Appl Supercond* 2012;22:5701105.
- [27] Dharmakeerthi CH, Mithulanthan N, Saha TK. Impact of electric vehicle fast charging on power system voltage stability. *Int J Electr Power Energy Syst* 2014;57:241–9.
- [28] Grigore A, Mao T, Berry A, Tan J, Purushothaman L, Mihaita A-S. How will electric vehicles affect traffic congestion and energy consumption: an integrated modelling approach. In: 2021 IEEE International Intelligent Transportation Systems Conference (ITSC); 2021. p. 1635–42.
- [29] Rigas ES, Ramchurn SD, Bassiliades N, Koutitas G. Congestion management for urban EV charging systems. In: 2013 IEEE International Conference on Smart Grid Communications (SmartGridComm); 2013. p. 121–6.
- [30] Jing W, Ramezani M, An K, Kim I. Congestion patterns of electric vehicles with limited battery capacity. *PLoS One* 2018;13:e0194354.
- [31] Marmaras C, Xydas E, Cipcigan L. Simulation of electric vehicle driver behaviour in road transport and electric power networks. *Transp Res Part C: Emerg Technol* 2017;80:239–56.
- [32] Wang T, Tang T-Q, Huang H-J, Qu X. The adverse impact of electric vehicles on traffic congestion in the morning commute. *Transp Res Part C: Emerg Technol* 2021;125.
- [33] Wang H, Meng Q, Wang J, Zhao D. An electric-vehicle corridor model in a dense city with applications to charging location and traffic management. *Transp Res B Methodol* 2021;149:79–99.
- [34] Cen X, Lo HK, Li L, Lee E. Modeling electric vehicles adoption for urban commute trips. *Transp Res B Methodol* 2018;117:431–54.
- [35] Huang C-J, Hu K-W, Ho HY, Xie BZ, Feng C-C, Chuang H-W. A distributed urban traffic congestion prevention mechanism for mixed flow of human-driven and autonomous electric vehicles. *Int J Comput Intell Syst* 2021;14:1714–27.
- [36] Solar Energy Laboratory of the University of Wisconsin-Madison. TRANNSOLAR Energietechnik GmbH, CSTB – Centre Scientifique et Technique du Bâtiment, TESS – Thermal Energy Systems Specialists. Section 8.7 Meteonorm data. Volume 8 Weather Data TRNSYS 18 document package. 2017.
- [37] Meteotest AG. Meteonorm. <https://meteonorm.com/en/>; 2025.
- [38] M. D. Hydrographic office. Hong Kong Tidal Stream Prediction System. <https://current.hydro.gov.hk/>; 2025.
- [39] Electrical & Mechanical services department (EMSD) the government of the Hong Kong special administrative region. Performance-Based Build Energy Code. 2007.
- [40] Tesla Motors. Model S. <https://www.tesla.com/models>; 2025.
- [41] Cao S. Comparison of the energy and environmental impact by integrating a H 2 vehicle and an electric vehicle into a zero-energy building. *Energy Convers Manag* 2016;123:153–73.
- [42] The University of Wisconsin Madison. TRNSYS – Official Website. <https://sel.me.wisc.edu/trnsys/features/features.html>; 2025.
- [43] Nicolas B, Marcotte B, Kummert M. Calling Python from TRNSYS with CFFI. Polytechnique Montréal 2022.
- [44] Global Wind Energy Council. Global wind report. 2024.
- [45] Li J, Wang G, Li Z, Yang S, Chong WT, Xiang X. A review on development of offshore wind energy conversion system. *Int J Energy Res* 2020;44:9283–97.
- [46] wind-turbine-models.com. Bonus B31/300. 2025 <https://en.wind-turbine-models.com/turbines/191-bonus-b31-300>.
- [47] Luo H, Cao S, Lu VL. The techno-economic feasibility of a coastal zero-energy hotel building supported by the hybrid wind-wave energy system. *Sustainable Energy, Grids Net* 2022;30:100650.
- [48] Kannan N, Vakesan D. Solar energy for future world: - A review. *Renew Sust Energ Rev* 2016;62:1092–105.
- [49] IEA. Renewables 2023. Paris: IEA; 2024. <https://www.iea.org/reports/renewables-2023>.
- [50] Sahu A, Yadav N, Sudhakar K. Floating photovoltaic power plant: A review. *Renew Sust Energ Rev* 2016;66:815–24.
- [51] FuturaSun. FU 260 P. https://www.futurasun.com/wp-content/uploads/2019/12/2020_FuturaSun_60p_260-285W_en.pdf?x97762; 2025.
- [52] Hammons TJ. Tidal power. *Proc IEEE* 1993;81:419–33.

- [53] Chowdhury MS, Rahman KS, Selvanathan V, Nuthammachot N, Suklueng M, Mostafaeipour A, et al. Current trends and prospects of tidal energy technology. *Environ Dev Sustain* 2021;23:8179–94.
- [54] Bin Abul Kashem SE, Majid M, Tabassum M, Ashraf A, Guziński J, Łuksza K. A preliminary study and analysis of tidal stream generators. *Acta Energetica* 2020; 6–22.
- [55] Hardisty J. The tidal stream power curve: A case study. *Energy Power Eng* 2012;04: 132–6.
- [56] Zhou S, Cao S, Wang S. Realisation of a coastal zero-emission office building with the support of hybrid ocean thermal, floating photovoltaics, and tidal stream generators. *Energy Convers Manag* 2022;253.
- [57] Cao S, Sirén K. Matching indices taking the dynamic hybrid electrical and thermal grids information into account for the decision-making of nZEB on-site renewable energy systems. *Energy Convers Manag* 2015;101:423–41.
- [58] HKSAR. EMSD. Feed-in Tariff (FiT). https://re.emsd.gov.hk/english/fit/int/fit_int.html; 2025.
- [59] The World Bank Group. Real interest rate (%) - Hong Kong SAR, China. <https://data.worldbank.org/indicator/FR.INR.RINR?locations=HK>; 2025.
- [60] IRENA. Renewable Power Generation Costs in 2022. <https://www.irena.org/Publications/2023/Aug/Renewable-Power-Generation-Costs-in-2022>; 2025.
- [61] Chen F. The Kuroshio power plant. Springer; 2013.
- [62] Hsieh I-YL, Pan MS, Chiang Y-M, Green WH. Learning only buys you so much: practical limits on battery price reduction. *Appl Energy* 2019;239:218–24.
- [63] CLP. Tariff 2023 FAQ. https://www.clp.com.hk/content/dam/clphk/documents/tariff-adjustment-20221/Tariff2023_FAQ_ENG.pdf; 2025.
- [64] CLP. CLP 2022 Sustainability Report. <https://sustainability.clpgroup.com/en/2022/>; 2025.